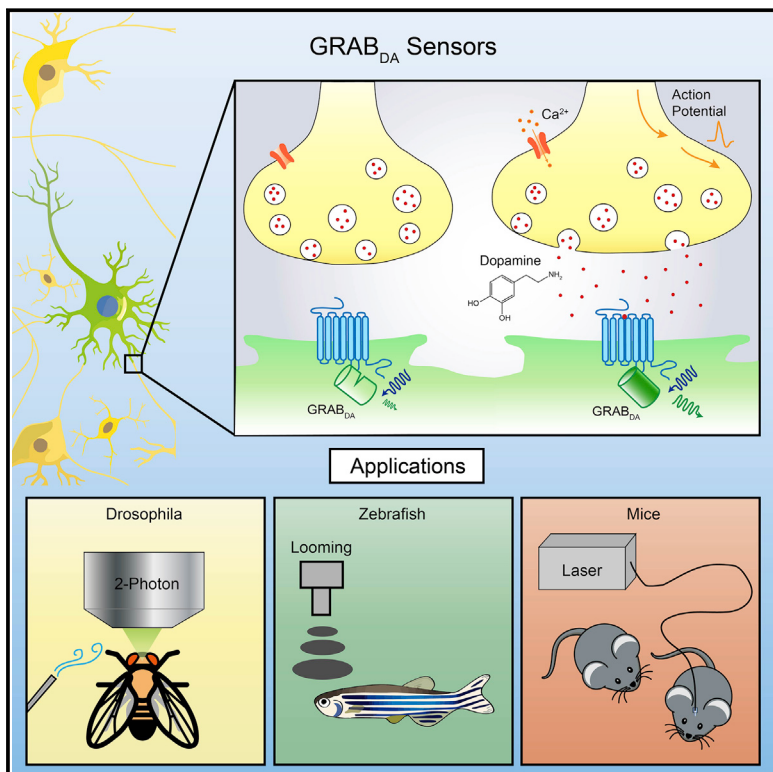


# A Genetically Encoded Fluorescent Sensor Enables Rapid and Specific Detection of Dopamine in Flies, Fish, and Mice

## Graphical Abstract



## Authors

Fangmiao Sun, Jianzhi Zeng,  
Miao Jing, ..., Anatol C. Kreitzer,  
Guohong Cui, Yulong Li

## Correspondence

yulongli@pku.edu.cn

## In Brief

The development of GPCR-activation-based-DA (GRAB<sub>DA</sub>) sensors enables measurements of dopamine dynamics in freely behaving animals with high spatiotemporal precision.

## Highlights

- GRAB<sub>DA</sub> sensors are genetically encoded dopamine (DA) sensors based on GPCR
- GRAB<sub>DA</sub> enables fast, sensitive DA detection with molecular and cellular specificity
- Two separate constructs expand the effective dynamic range of DA detection
- Sensors report DA dynamics *in vivo* in multiple organisms and during complex behaviors



# A Genetically Encoded Fluorescent Sensor Enables Rapid and Specific Detection of Dopamine in Flies, Fish, and Mice

Fangmiao Sun,<sup>1,2,13</sup> Jianzhi Zeng,<sup>1,2,3,13</sup> Miao Jing,<sup>1,2,3,13</sup> Jingheng Zhou,<sup>4</sup> Jiesi Feng,<sup>1,2,3</sup> Scott F. Owen,<sup>5</sup> Yichen Luo,<sup>1</sup> Funing Li,<sup>6,10</sup> Huan Wang,<sup>1,2</sup> Takashi Yamaguchi,<sup>7</sup> Zihao Yong,<sup>2,3,8</sup> Yijing Gao,<sup>7</sup> Wanling Peng,<sup>6</sup> Lizhao Wang,<sup>9</sup> Siyu Zhang,<sup>9</sup> Jiulin Du,<sup>6,10</sup> Dayu Lin,<sup>7,11</sup> Min Xu,<sup>6</sup> Anatol C. Kreitzer,<sup>5,12</sup> Guohong Cui,<sup>4</sup> and Yulong Li<sup>1,2,3,14,\*</sup>

<sup>1</sup>State Key Laboratory of Membrane Biology, Peking University School of Life Sciences, 100871 Beijing, China

<sup>2</sup>PKU-IDG/McGovern Institute for Brain Research, 100871 Beijing, China

<sup>3</sup>Peking-Tsinghua Center for Life Sciences, 100871 Beijing, China

<sup>4</sup>Neurobiology Laboratory, National Institute of Environmental Health Sciences, National Institutes of Health, Research Triangle Park, NC 27709, USA

<sup>5</sup>Gladstone Institutes, San Francisco, CA 94158, USA

<sup>6</sup>Institute of Neuroscience, State Key Laboratory of Neuroscience, CAS Center for Excellence in Brain Science and Intelligence Technology, Chinese Academy of Sciences, 200031 Shanghai, China

<sup>7</sup>Neuroscience Institute, New York University School of Medicine, New York, NY 10016, USA

<sup>8</sup>College of Biological Sciences, China Agricultural University, 100193 Beijing, China

<sup>9</sup>Shanghai Jiao Tong University School of Medicine, 200025 Shanghai, China

<sup>10</sup>University of Chinese Academy of Sciences, 100049 Beijing, China

<sup>11</sup>Department of Psychiatry, New York University School of Medicine, New York, NY 10016, USA

<sup>12</sup>Department of Neurology, Kavli Institute for Fundamental Neuroscience, Weill Institute for Neurosciences, Department of Physiology, University of California, San Francisco, CA 94158, USA

<sup>13</sup>These authors contributed equally

<sup>14</sup>Lead Contact

\*Correspondence: [yulongli@pku.edu.cn](mailto:yulongli@pku.edu.cn)

<https://doi.org/10.1016/j.cell.2018.06.042>

## SUMMARY

Dopamine (DA) is a central monoamine neurotransmitter involved in many physiological and pathological processes. A longstanding yet largely unmet goal is to measure DA changes reliably and specifically with high spatiotemporal precision, particularly in animals executing complex behaviors. Here, we report the development of genetically encoded GPCR-activation-based-DA (GRAB<sub>DA</sub>) sensors that enable these measurements. In response to extracellular DA, GRAB<sub>DA</sub> sensors exhibit large fluorescence increases ( $\Delta F/F_0 \sim 90\%$ ) with subcellular resolution, subsecond kinetics, nanomolar to submicromolar affinities, and excellent molecular specificity. GRAB<sub>DA</sub> sensors can resolve a single-electrical-stimulus-evoked DA release in mouse brain slices and detect endogenous DA release in living flies, fish, and mice. In freely behaving mice, GRAB<sub>DA</sub> sensors readily report optogenetically elicited nigrostriatal DA release and depict dynamic mesoaccumbens DA signaling during Pavlovian conditioning or during sexual behaviors. Thus, GRAB<sub>DA</sub> sensors enable spatiotemporally precise measurements of DA dynamics in a variety of model organisms while exhibiting complex behaviors.

## INTRODUCTION

Dopamine (DA) is a crucial monoamine neurotransmitter across many species. In the vertebrate central nervous system, DA regulates a wide range of complex processes, including reward signaling (Schultz, 2016; Wise, 2004), reinforcement learning (Holroyd and Coles, 2002), attention (Nieoullon, 2002), and motor control (Graybiel et al., 1994). In the human brain, impaired DA transmission is associated with neurological diseases, including ADHD (Cook et al., 1995), schizophrenia (Howes and Kapur, 2009), and Parkinson's disease (Lotharius and Brundin, 2002). In addition, psychostimulants like cocaine act by altering extracellular DA levels in the brain to exert addictive effects (Di Chiara and Imperato, 1988).

Despite these important roles for DA, precise measurements of the spatial and temporal patterns of DA release during complex behaviors are lacking due in large part to the limitations of existing methods for DA detection. Intracerebral microdialysis has long been the gold standard for quantitative measurements of extracellular DA concentration. However, its relatively slow sampling rate (>1 min between sampling, typically ~10 min) (Chefer et al., 2009) is not well suited to detect DA dynamic changes during complex and rapidly evolving behaviors (Tidey and Miczek, 1996). Fast-scan cyclic voltammetry (FSCV) is an electrochemical method that can measure changes in extracellular DA concentrations with 10 ms temporal resolution and ~1 nM sensitivity (Robinson et al., 2008). However, FSCV requires substrate oxidization for signal detection; therefore, it



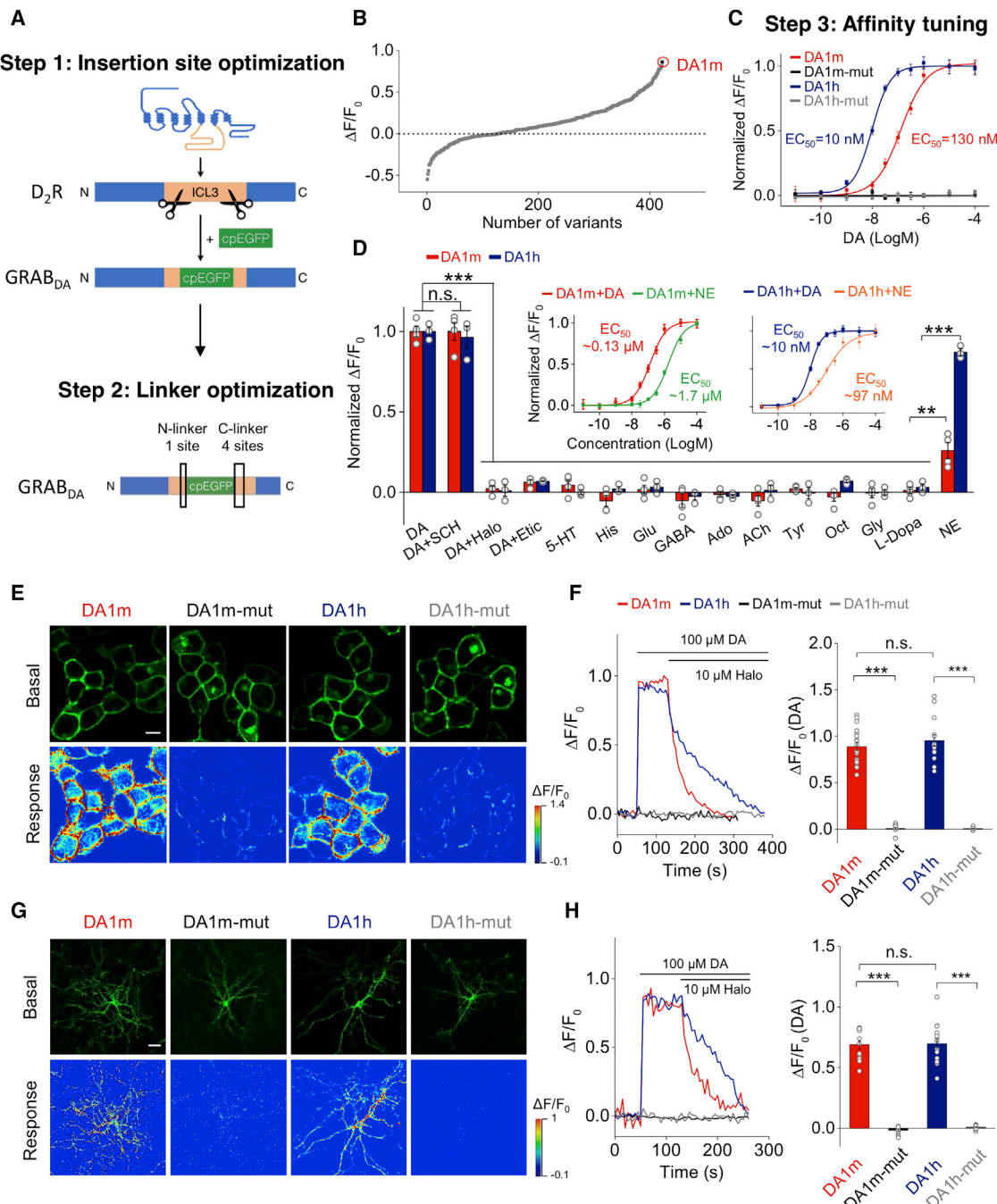


**Figure 1. Design, Optimization, and Characterization of GRAB<sub>DA</sub> Sensors in HEK293T Cells and Cultured Neurons**

(A) Schematic diagrams showing the strategy of insertion site and linker optimization.

(B) Optimization of the cpEGFP insertion site within the third intracellular loop (ICL3) of D<sub>2</sub>R and the linkers between D<sub>2</sub>R and cpEGFP. The fluorescence responses of variant-expressing cells in response to 100-μM DA application are shown. DA1m, with the highest ΔF/F<sub>0</sub>, was selected for further optimization. Each point represents the average of at least three to five cells.

(C) Affinity tuning. Either the T205M single mutation (generating DA1h) or the C118A/S193N double mutations (generating DA1m/h-mut) were introduced into DA1m. The normalized dose-dependent fluorescence responses of various GRAB<sub>DA</sub>-expressing cells in response to DA application are plotted. Each point represents average of six wells containing 100–400 cells per well.

(D) Normalized fluorescence changes in DA1m (red)- and DA1h (blue)-expressing cells in response to the application of indicated compounds at 1 μM: DA, DA + SCH, DA + Halo, DA + Etic, 5-HT, histamine (His), glutamate (Glu), gamma-aminobutyric acid (GABA), adenosine (Ado), acetylcholine (ACh), tyramine (Tyr), octopamine (Oct), glycine (Gly), L-DOPA and NE (DA1m: n = 4 wells; DA1h: n = 3 wells; 200–400 cells per well; p > 0.05 for DA1m/h responses induced by DA compared with DA+SCH; p < 0.001 for DA1m/h responses induced by DA compared with DA+Halo, DA+Etic, 5-HT, His, Glu, GABA, Ado, ACh, Tyr, Oct, Gly, and NE).

(legend continued on next page)

is not readily able to distinguish DA from other structurally similar neurotransmitters, such as norepinephrine (NE) (Robinson et al., 2003). Moreover, both microdialysis and FSCV require implantation of a relatively large probe (approximately 70–300  $\mu\text{m}$  in diameter) into brain tissue, which limits the ability to achieve spatially precise measurements of endogenous DA release (Jaquins-Gerstl and Michael, 2015).

In lieu of direct measurements, indirect methods, such as measuring the activation of downstream targets of DA receptors, have been used to approximate the dynamics of DA. Cell-based DA reporters, such as CNiFERS (Muller et al., 2014), use transplanted HEK293 cells constitutively expressing DA receptors together with an intracellular  $\text{Ca}^{2+}$  indicator to couple extracellular DA signals to fluorescence changes. Despite its high sensitivity, this approach requires cell transplantation and only reports the volume transmission of DA. The TANGO assay, as well as next-generation versions (Barnea et al., 2008; Inagaki et al., 2012; Kim et al., 2017; Lee et al., 2017), have been used to measure endogenous DA release by coupling the  $\beta$ -arrestin signaling pathway to the expression of reporter genes. Although this approach enables cell-type-specific expression of DA reporters and is suitable for *in vivo* measurements, the long signal amplification time (on the order of hours) precludes the ability to monitor rapid, physiologically relevant dynamics of DA signaling.

Here, we report the development of genetically encoded fluorescent sensors for direct, rapid, sensitive, and cell-type-specific detection of extracellular DA. These sensors, which we call GRAB<sub>DA</sub> (G protein-coupled receptor [GPCR]-activation-based DA) sensors, were engineered by coupling a conformationally sensitive circular-permuted EGFP (cpEGFP) to a selected human DA receptor. Through iterative engineering and optimization, we arrived at two GRAB<sub>DA</sub> sensors: GRAB<sub>DA1m</sub> (abbreviated to DA1m), with medium apparent affinity to DA ( $\text{EC}_{50}\sim 130 \text{ nM}$ ); and GRAB<sub>DA1h</sub> (abbreviated to DA1h), with high apparent affinity to DA ( $\text{EC}_{50}\sim 10 \text{ nM}$ ). These two sensors enable real-time detection of endogenous DA in acute brain slices of mice and in the intact brains of versatile animal models including flies, fish, and mice.

## RESULTS

### Development and Characterization of GRAB<sub>DA</sub> Sensors in HEK293T Cells and Cultured Neurons

To develop a genetically encoded sensor for DA, we started with natural DA receptors as the sensing module and coupled a cpEGFP as a fluorescent light output module. We hypothesized that upon DA binding, the conformational changes in the receptor could alter the arrangement of the associated cpEGFP,

resulting in a DA-dependent change in fluorescence. Indeed, a similar strategy was recently applied in creating the genetically encoded acetylcholine sensor GACh (Jing et al., 2018).

We used a three-step approach to engineer GRAB<sub>DA</sub> sensors (Figure 1A). First, a cpEGFP was inserted into the third intracellular loop (ICL3) of each human DA receptor subtype (DR). Based on preliminary results, we subsequently focused on the D<sub>2</sub>R-cpEGFP chimera due to its superior membrane trafficking and high affinity for DA (Beaulieu and Gainetdinov, 2011; Missale et al., 1998) (Figure S1A). Second, the position of the cpEGFP insertion and the linker residues were systematically screened (Figures 1A and 1B). Finally, mutations were introduced to expand the response range (Figure 1C). After screening, we chose two variants, DA1m and DA1h, for further characterization. Both sensors have ~90% maximal  $\Delta F/F_0$  responses to DA with ~70% brightness of EGFP (Figures 1E, 1F, and S1B) but differ by an order of magnitude with respect to apparent affinity for DA ( $\text{EC}_{50}$  130 nM for DA1m and 10 nM for DA1h) (Figure 1C). We also generated DA-insensitive control sensors containing the mutations C118A and S193N in the DA-binding pocket (Figures 1C and 1E–1H) that prevent the sensor from DA binding.

We next expressed GRAB<sub>DA</sub> sensors in HEK293T cells and cultured neurons for further characterization. GRAB<sub>DA</sub> sensors trafficked efficiently to the plasma membrane (Figures 1E, 1G, and S1), and fluorescent signals were clearly distinguishable in subcellular compartments in neurons (Figures S1F and S1G). Both DA1m and DA1h exhibited robust fluorescence increases to DA, which could be blocked by co-application of D<sub>2</sub>R antagonist haloperidol (Halo) (Sokoloff et al., 1990) (Figures 1F and 1H). Mutant sensors (DA1m/h-mut) did not show detectable fluorescence increases to DA application (Figures 1E–1H).

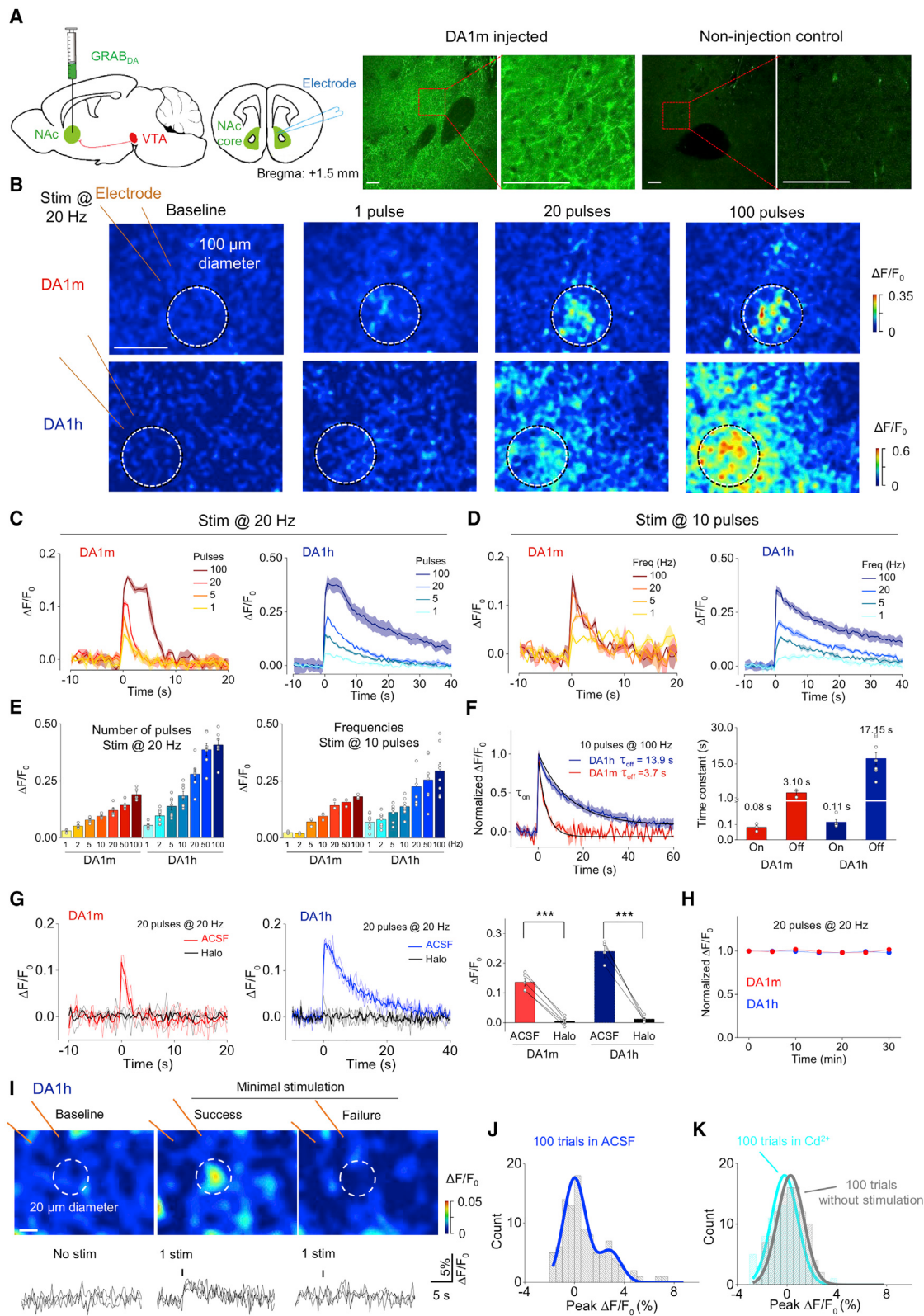
GRAB<sub>DA</sub> sensors exhibited photostability similar to or better than EGFP or other cpEGFP-based sensors (Figure S1C). Using a local perfusion system, both DA1m and DA1h showed rapid fluorescence increases (on rate) to DA application (Figures S1D and S1E;  $60 \pm 10 \text{ ms}$  for DA1m and  $140 \pm 20 \text{ ms}$  for DA1h). The fluorescence decrease (off rate) in response to application of the antagonist Halo is slower in DA1h ( $2.5 \pm 0.3 \text{ s}$ ) compared with DA1m ( $0.7 \pm 0.06 \text{ s}$ ), consistent with the differences in  $\text{EC}_{50}$ . For the specificity, bath application of DA elicited robust fluorescence increase in GRAB<sub>DA</sub> sensors-expressing cells, which were completely blocked by co-application of D<sub>2</sub>R antagonists Halo or eticlopride (Etic), but not by the D<sub>1</sub>R antagonist SCH-23390 (SCH) (Figure 1D). In addition, application of several other neurotransmitters did not elicit any detectable fluorescence changes, except for NE, which drove modest fluorescence increase (Figure 1D). Further characterization

L-DOPA; p = 0.004 for DA1m and p < 0.001 for DA1h, comparing responses induced by NE with L-Dopa). The insets show the normalized dose-dependent responses of DA1m- or DA1h-expressing cells to DA and NE application (n = 6 wells per group with 200–400 cells per well).

(E and F) Expression of GRAB<sub>DA</sub> sensors in HEK293T cells. (E) Representative basal fluorescence intensity (without DA) and responses to 100  $\mu\text{M}$  DA. (F) Representative traces and group analysis of fluorescence changes in GRAB<sub>DA</sub>-expressing cells in response to 100  $\mu\text{M}$  DA followed by 10  $\mu\text{M}$  Halo (DA1m: n = 18 cells from 4 cultures [18/4]; DA1m-mut: n = 15/3; DA1h: n = 14/3; DA1h-mut: n = 14/3; p < 0.001 between DA1m and DA1m-mut; p < 0.001 between DA1h and DA1h-mut; p = 0.42 between DA1m and DA1h).

(G and H) Similar to (E) and (F) except that GRAB<sub>DA</sub> sensors are expressed in cultured neurons (DA1m: n = 13/7; DA1m-mut: n = 14/5; DA1h: n = 16/4; DA1h-mut: n = 10/5; p < 0.001 between DA1m and DA1m-mut; p < 0.001 between DA1h and DA1h-mut; p = 0.88 between DA1m and DA1h).

Scale bars, 10  $\mu\text{m}$  (E) and 30  $\mu\text{m}$  (G). Values with error bars indicate mean  $\pm$  SEM. Students' t test performed; n.s., not significant; \*\*p < 0.01; \*\*\*p < 0.001. See also Figures S1 and S2.



(legend on next page)

of the dose-dependent responses to DA and NE revealed a ~10-fold lower EC<sub>50</sub> to DA than NE (Figures 1D, insets, and S2A–S2D). Thus, both DA1h and DA1m are selective for DA over NE at physiological concentrations (DA: 10–100 nM; NE: 1–100 nM) (Bungay et al., 2003; Florin-Lechner et al., 1996; Pacak et al., 1995; Schultz, 2007; Smith et al., 1992). Overall, both sensors show rapid and sensitive responses to physiological ranges of DA with little or no crosstalk to other neurotransmitters.

To test the coupling of GRAB<sub>DA</sub> sensors to GPCR downstream pathways, we examined the coupling efficacies of GRAB<sub>DA</sub> sensors to either G protein- or β-arrestin-dependent pathways (Beaulieu and Gainetdinov, 2011). Application of DA largely reduced the forskolin-induced cAMP increases in wild-type (WT)-D<sub>2</sub>R-expressing cells, but not in DA1h-expressing cells (Figure S2E). Furthermore, co-expression of pertussis toxin (PTX) or GTPγS treatment did not alter the EC<sub>50</sub> to DA for DA1m and DA1h sensors (Figures S2F and S2G), suggesting the negligible coupling of GRAB<sub>DA</sub> sensors to downstream G protein signaling. Next, we measured DA-induced internalization to indicate the coupling with β-arrestin pathway (Luttrell and Lefkowitz, 2002). Compared with WT-D<sub>2</sub>R that underwent rapid decrease of membrane fluorescence signals within 10 min, GRAB<sub>DA</sub> sensors showed stable membrane fluorescence signals throughout 2-hr DA exposure (Figures S2H and S2I). In addition, DA1h-expressing cells showed less β-arrestin-dependent reporter signal in the TANGO assay compared with WT-D<sub>2</sub>R-expressing cells (Figure S2J). Collectively, these data suggest that GRAB<sub>DA</sub> sensors do not engage the primary signaling pathways downstream of D<sub>2</sub>R.

### Imaging DA Dynamics in Acute Brain Slices

To monitor endogenous DA release by GRAB<sub>DA</sub> sensors, we virally expressed DA1m or DA1h by adeno-associated virus (AAV) into nucleus accumbens (NAc) of mice and prepared acute

brain slices 2 weeks later. Strong fluorescence signals were detected in sensor-expressing slices, but not in uninjected control slices. Sensor fluorescence was in close proximity with tyrosine hydroxylase (TH)-labeled dopaminergic fibers (Figures 2A and S4A). Electrical stimulation of NAc core elicited transient fluorescence increases (Figures 2A–2E and S4B–S4D and Video S1). The rising time constants of signals were fast (~0.1 s) for both DA1m and DA1h (Figure 2F), whereas the decaying time constant of DA1h (~17 s) was slower than DA1m (~3 s) (Figure 2F). Bath application of Halo abolished the evoked responses (Figure 2G), verifying the signal specificity. Responses to repeated stimulation trains were stable over 30 min of recording (Figure 2H).

To test whether these sensors could sensitively report DA release from single dopaminergic fibers, we conducted minimal stimulation experiments (Balaji and Ryan, 2007; Allen and Stevens, 1994). We prepared acute slices of NAc expressing DA1h (Figure S3A) and gradually turned down the stimulation strength until >50% of response failures occurred. We then repeated 100 trials at this stimulus strength in normal artificial cerebrospinal fluid (ACSF) followed by 100 trials in ACSF containing 200 μM Cd<sup>2+</sup> (Mintz et al., 1995) (Figures 2I–2K and S3B–S3E). Trials without stimulation and stimulation trials in the presence of Cd<sup>2+</sup> exhibited a single peak in the distribution of responses at ~0% ΔF/F<sub>0</sub> (Figures 2K, S3E, and S3F). In contrast, responses in control ACSF showed a bimodal distribution, with an additional peak shifted by ~3% ΔF/F<sub>0</sub> (Figures 2J, S3B, S3G, and S3H). This second peak represents the signal of DA release from putative activation of single fibers.

### Imaging DA Dynamics in *Drosophila*

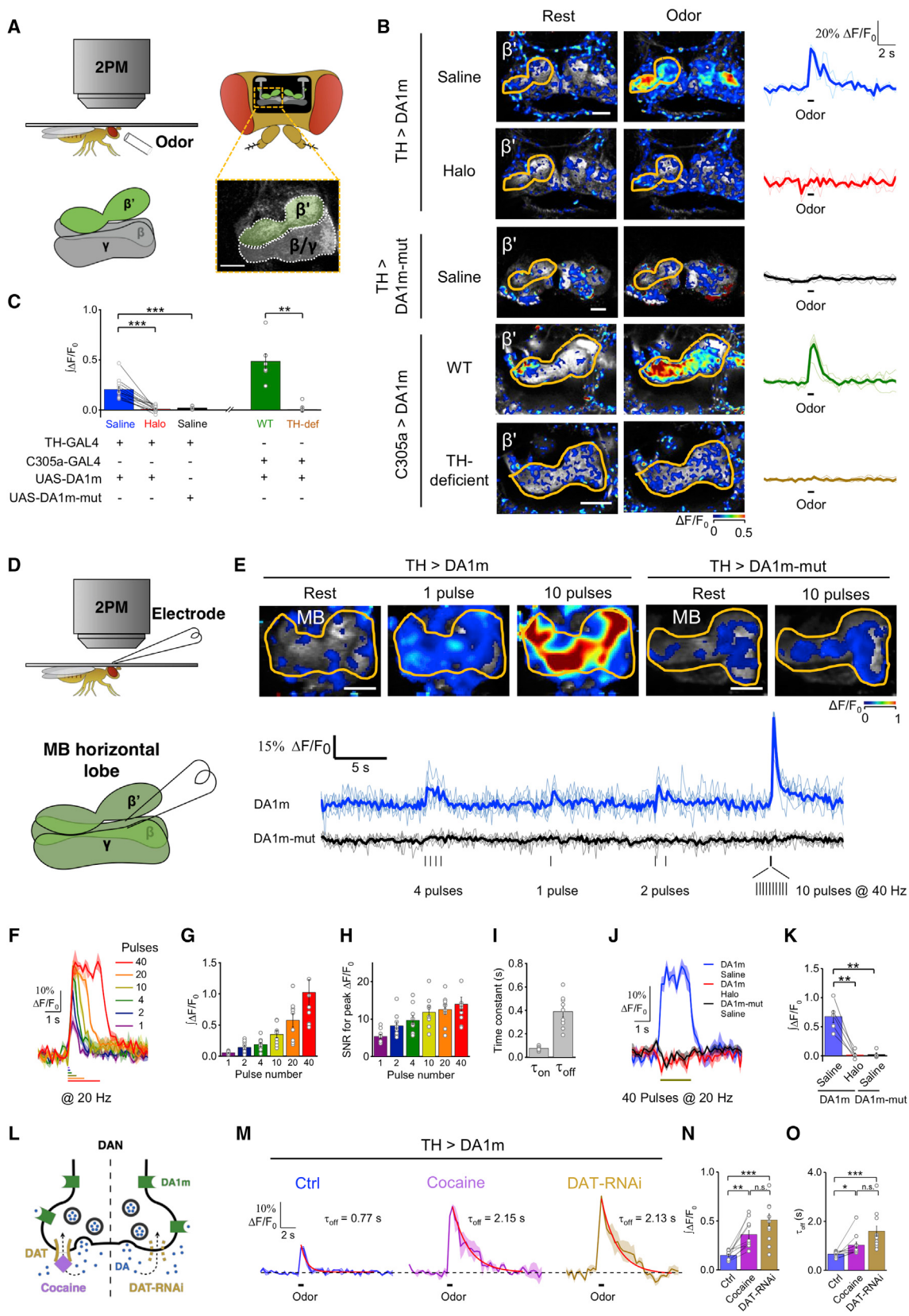
To test the ability of GRAB<sub>DA</sub> sensors to detect physiologically relevant DA dynamics in living animals, we started with *Drosophila*, because DA serves as a critical teaching signal in olfactory-associative learning in the fly brain (Burke et al.,

### Figure 2. Release of Endogenous DA Measured in Acute Mouse Brain Slices

- (A) Left two panels: schematic of the experimental protocol for expressing GRAB<sub>DA</sub> sensors and imaging DA dynamics in mouse brain slices containing NAc. Right: the immunoreactive signals of GFP in NAc slices from either DA1m injected or non-injection control mice. Red squares in left panel indicate expanded region in right panel. Scale bars, 100 μm.
- (B) Representative pseudocolor images of fluorescence responses in DA1m- or DA1h-expressing neurons following 20 Hz of electrical stimulation containing the indicated pulse numbers. White circles represent the region of interest (ROI) selected for analysis. Scale bar, 100 μm.
- (C and D) Representative fluorescence responses of DA1m- and DA1h-expressing neurons following 20-Hz electrical stimuli containing the indicated pulse numbers (C) or a 10-pulse-train electrical stimulation at the indicated frequencies (D). Each trace is the average of three trials in one slice.
- (E) Group analysis of the fluorescence responses to electrical stimuli at different pulse numbers or frequencies (pulses: DA1m: n = 5 slices from 3 mice; DA1h: n = 7 slices from 4 mice. Frequencies: DA1m: n = 3 slices from 2 mice; DA1h: n = 8 slices from 4 mice).
- (F) Representative traces (left) and group analysis (right) of the normalized fluorescence changes and kinetics in DA1m- and DA1h-expressing neurons to 10 electrical pulses delivered at 100 Hz. The rising (on) and decaying (off) phases are fitted and summarized on the right (DA1m: n = 3 slices from 2 mice; DA1h: n = 5–8 slices from 3 mice).
- (G) Representative traces (left and middle, with three individual trials and the averaged trials) and group analysis (right) of DA1m- and DA1h-expressing neurons to 20 electrical pulses at 20 Hz in control solution (ACSF) or solution containing 10 μM Halo (DA1m: n = 5 slices from 4 mice, p < 0.001 comparing ACSF with Halo; DA1h: n = 6 slices from 4 mice, p < 0.001 comparing ACSF with Halo).
- (H) The fluorescence changes in DA1m- and DA1h-expressing neurons to multiple trains of electrical stimuli with an interval of 5 min. The fluorescence changes induced by the first train were used to normalize the data in each slice (DA1m: n = 3 slices from 2 mice; DA1h: n = 6 slices from 3 mice).
- (I) Top: representative pseudocolor images of fluorescence responses during minimal stimulation (left, baseline; middle, success trial; right, failure trial). White circles represent ROI with ~20-μm diameter. Bottom: three exemplar trials for each condition, with the black ticks indicating the stimulation. The data were processed with 3× binning. Scale bar, 10 μm.
- (J) The distribution of peak ΔF/F<sub>0</sub> of DA1h-expressing neurons in 100 minimal-stimulation trials in ACSF.
- (K) Comparison of the distribution of peak ΔF/F<sub>0</sub> in 100 trials without stimulation in ACSF (gray) and with stimulation in ACSF containing Cd<sup>2+</sup> (light blue) from the same slice.

Values with error bars or shaded areas indicate mean ± SEM. Student's t test performed; \*\*\*p < 0.001.

See also Figures S3 and S4 and Video S1.



(legend on next page)

2012; Davis, 1993; Heisenberg, 2003; Liu et al., 2012; Schwaerzel et al., 2003). Transgenic UAS-DA1m flies were generated and crossed with TH-GAL4 to express DA1m specifically in dopaminergic neurons (DANs) (Figure 3A). Under two-photon imaging, the odor isoamyl acetate (IA) elicited time-locked fluorescence increases in the mushroom body (MB), most prominently in the  $\beta'$  lobes (Video S2), and the odor-evoked responses were blocked by Halo application. In contrast, no odor-evoked fluorescence response was observed in flies expressing DA1m-mut. When we expressed DA1m in Kenyon cells, which receive direct input from DANs (Aso et al., 2014; Mao and Davis, 2009; Tanaka et al., 2008), we observed odor-evoked responses in WT flies, but not in TH-deficient flies that lack DA synthesis, validating the specificity of the signals (Figures 3B and 3C) (Ciche-wicz et al., 2017).

To further characterize the sensitivity and kinetics of DA1m *in vivo*, we electrically stimulated MB DANs while imaging the MB horizontal lobe (Figure 3D). We found that DA1m-expressing DANs, instead of DA1m-mut-expressing DANs, exhibited reproducible fluorescence increases in response to electrical stimulation, and single stimulus was sufficient to elicit a measurable fluorescence increase (Figures 3E–3K and S4E–S4G). Response kinetics were subsecond (Figure 3I), and responses were completely blocked by the Halo application (Figures 3J, 3K, and S4G).

Within the MB  $\gamma$  lobe of DA1m-expressing flies (Figure S5A), we observed that odor selectively elicited responses in the  $\gamma 4$  compartment (Figure S5Bi), while aversive electrical shock to the abdomen evoked responses in the  $\gamma 2$  and  $\gamma 3$  compartments (Figure S5Bii). As a control, exogenous DA application caused overall fluorescence increases in  $\gamma 2$ – $\gamma 5$  compartments (Figure S5Biii). These results provide direct evidence of compartmentalized DA dynamics during sensory processing in the MB as postulated by indirect presynaptic  $\text{Ca}^{2+}$  imaging of DAN (Berry et al., 2012; Cohn et al., 2015).

To explore whether DA1m is sensitive and bright enough to report DA signals perceived by a single neuron *in vivo*, we

adopted MB296B-GAL4 to express DA1m in one DAN per hemisphere innervating MB  $\gamma 2$  compartment (Aso et al., 2014; Tanaka et al., 2008) (Figure S5C). A brief aversive electrical shock to the fly's abdomen elicited rapid, repeatable fluorescence rises in the  $\gamma 2$  compartment (Figures S5C–S5E), suggesting DA1m's feasibility for single-cell imaging.

The DA transporter (DAT) is critical in regulating extracellular DA levels and serves as a primary target for drugs of abuse, including cocaine (Figure 3L) (Bainton et al., 2000; Ritz et al., 1987). Indeed, cocaine application potentiated the odor-evoked responses in MB  $\beta'$  lobes of TH > DA1m flies and also prolonged the decay of signals. Knocking down the expression of DAT selectively in DANs phenocopied the effect of cocaine administration (Figures 3M–3O and S4H). Taken together, these data demonstrated that GRAB<sub>DA</sub> sensors have sufficient sensitivity, kinetics, and specificity to report *in vivo* DA dynamics with subcellular spatial resolution and subsecond temporal resolution in genetically defined neurons of living flies.

Finally, we examined whether the ectopic expression of DA1m alters physiological properties of neurons. We observed no significant difference of odor-evoked  $\text{Ca}^{2+}$  signals in either DANs or Kenyon cells between the flies with or without expression of DA1m (Figures S5F–S5H), suggesting that expression of the DA1m does not alter odor-evoked responses in neurons in the fly brain.

### Imaging DA Release in the Intact Zebrafish Brain

The larval zebrafish has an optically transparent brain and can perform a wide range of behaviors, making them a powerful system to explore the structure and function of the vertebrate brain at cellular resolution. To test the feasibility of using GRAB<sub>DA</sub> sensors in zebrafish larvae, we generated the transgenic line in which DA1m was expressed pan-neuronally throughout the brain, while TRPV1-TagRFP was expressed specifically in DANs to enable their chemogenetic activation by capsaicin (Figure 4A). Exogenous DA application caused a fluorescence increase in DA1m-expressing neurons that was blocked by

### Figure 3. *In Vivo* Imaging of DA Dynamics in the *Drosophila* Brain

- (A) Schematic for odor stimulation during two-photon microscopy in *Drosophila*.
- (B and C) Fluorescence changes of DA1m- or DA1m-mut-expressing flies to 1 s of odor stimulation. (B) Representative pseudocolor images, single-trial traces (light), and averaged traces (bold) from one fly. (C) Group analysis of the odor-evoked fluorescence responses (TH > DA1m: n = 12 flies; TH > DA1m-mut: n = 5 flies; C305a > DA1m WT flies: n = 6 flies; C305a > DA1m TH-deficient flies: n = 6 flies; p < 0.001 for TH > DA1m in saline compared with Halo; p < 0.001 for TH > DA1m compared with TH > DA1m-mut in saline; p = 0.002 for C305a > DA1m in WT flies compared with TH-deficient flies).
- (D) Schematic depicting *in vivo* electrical stimulation in which an electrode was positioned near the DA1m-expressing DANs in order to evoke DA release.
- (E) Top, representative pseudocolor images of TH > DA1m and TH > DA1m-mut flies in response to multiple trains of electrical pulses. Bottom, single-trial traces (light) and six-trial averaged traces (bold) from one fly with indicated genotypes. Each vertical tick indicates a 1-ms electrical pulse.
- (F–I) Electrical stimulation of TH > DA1m flies. Representative traces (F), group analysis of integrated signal (G), signal-to-noise ratios (H, SNR), and kinetics of responses to electrical pulses (I, n = 9 flies per group).
- (J and K) Fluorescence changes in TH > DA1m and TH > DA1m-mut flies in response to 40 pulses of electrical stimuli (at 20 Hz) in normal saline or in saline containing 10  $\mu\text{M}$  Halo (TH > DA1m: n = 5 flies; TH > DA1m-mut: n = 5 flies; p = 0.004 for responses of TH > DA1m in saline compared with Halo; p = 0.007 for responses of TH > DA1m in saline compared with TH > DA1m-mut in saline). Representative traces (J) and group analysis (K).
- (L–O) Fluorescence changes in TH > DA1m flies in response to 1 s of odor stimulation, in saline, saline containing 3  $\mu\text{M}$  cocaine, or when the DAT expression in DAN was impaired by DAT-RNAi. (L) Schematic of the experimental design. (M) Representative traces fitted with a single-exponential function (red traces), with the decay time constants shown. (N and O) The group analysis of integrals and the decay time constants (TH > DA1m: n = 10 flies; TH > DA1m, DAT-RNAi: n = 11 flies; between control and cocaine groups, p = 0.002 for integrals and p = 0.025 for decay time constants; between control and DAT-RNAi groups, p < 0.001 for both integrals and decay time constants; between cocaine and DAT-RNAi groups, p = 0.095 for integrals and p = 0.053 for decay time constants). Averaged traces shaded with  $\pm$  SEM are shown in (F), (J), and (M). Values with error bars indicate mean  $\pm$  SEM. Student's t test performed; n.s., not significant; \*p < 0.05; \*\*p < 0.01; \*\*\*p < 0.001. Scale bars in (B) and (E), 25  $\mu\text{m}$ .

See also Figures S4 and S5 and Video S2.

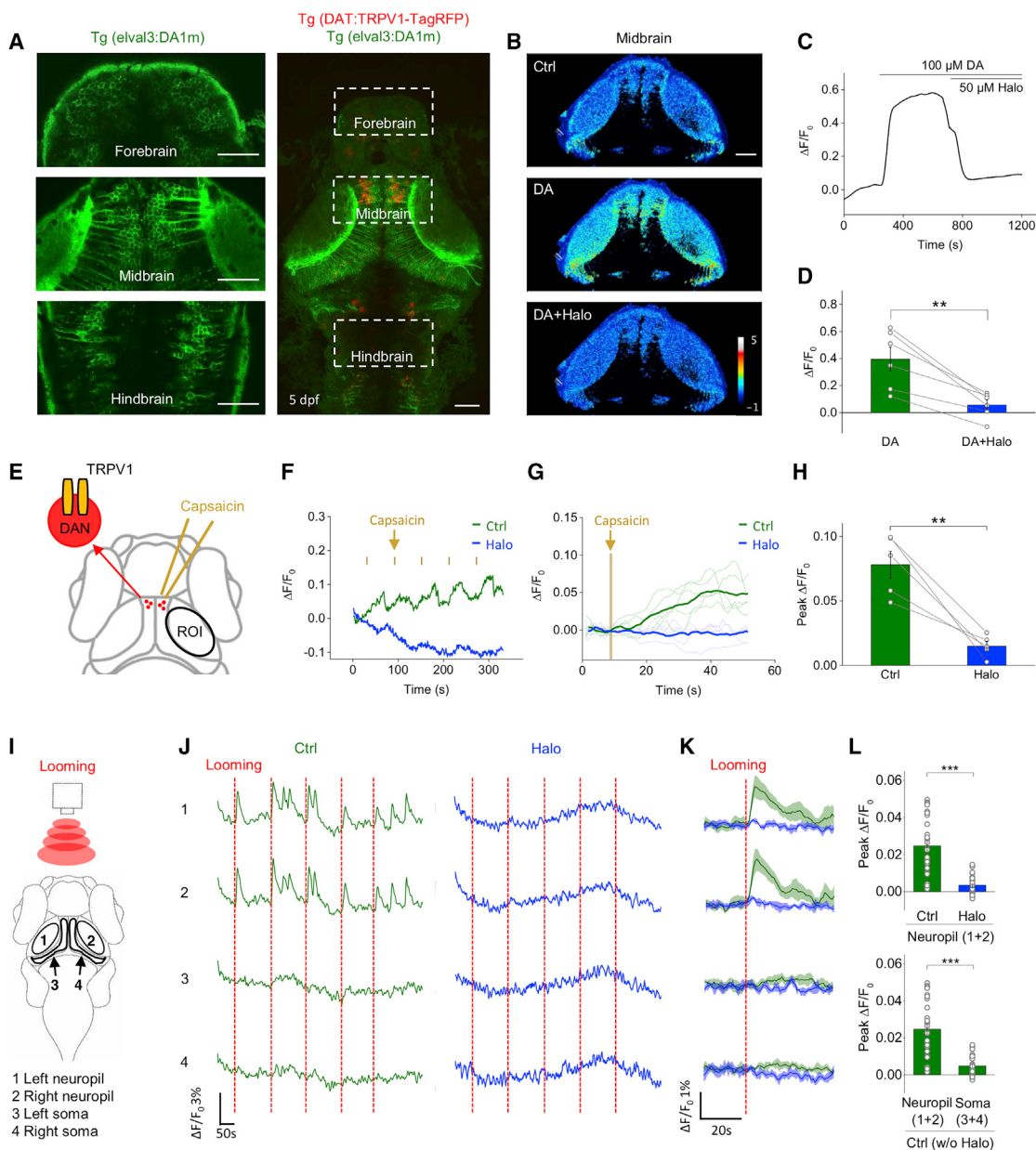


**Figure 4. Monitoring *In Vivo* DA Release in Transgenic Zebrafish**

(A) Fluorescence images of a transgenic zebrafish larva expressing DA1m (green) pan-neuronally and TRPV1-TagRFP (red) in DANs with expanded views of DA1m-expressing neurons in indicated brain regions (left).

(B–D) DA1m-expressing neurons to 100 μM DA followed by 50 μM Halo ( $n = 6$  fish;  $p = 0.002$  between DA and DA+Halo). (B) Representative pseudocolor images.

(C) Traces.

(D) Group analysis.

(E) Schematic of chemogenetic activation of TRPV1-expressing DANs by capsaicin. The fluorescence signals in the tectal neurons (within ROI) were analyzed.

(F–H) Fluorescence changes of DA1m-expressing neurons to five-trial capsaicin application in control solution (green) or solution containing 50 μM Halo (blue). Representative traces encompassing 5 sequential stimulation trials and corresponding averaged traces from one fish are shown in (F) and (G). (H) Group analysis ( $n = 5$  fish;  $p = 0.006$  between control and Halo).

(I) Schematic for visual stimulation in which red expanding dots were projected in front of the larva. The fluorescence responses in neuropil (1 and 2) and soma (3 and 4) regions of the optic tectum were analyzed, respectively.

(J–L) Fluorescence changes of DA1m-expressing neurons from each region during visual stimulation in control solution (green) or solution containing 50 μM Halo (blue). Vertical dashed red line, 3-s looming stimulation. Representative traces encompassing five sequential stimulation trials and the corresponding averaged traces from one fish are shown in (J) and (K). Group analysis is shown in (L) ( $n = 30$  trials from 3 fish for each condition;  $p < 0.001$  in two panels).

Scale bars in (A) and (B), 50 μm. Values with error bars indicate mean ± SEM. Student's t test performed; \*\* $p < 0.01$ ; \*\*\* $p < 0.001$ .

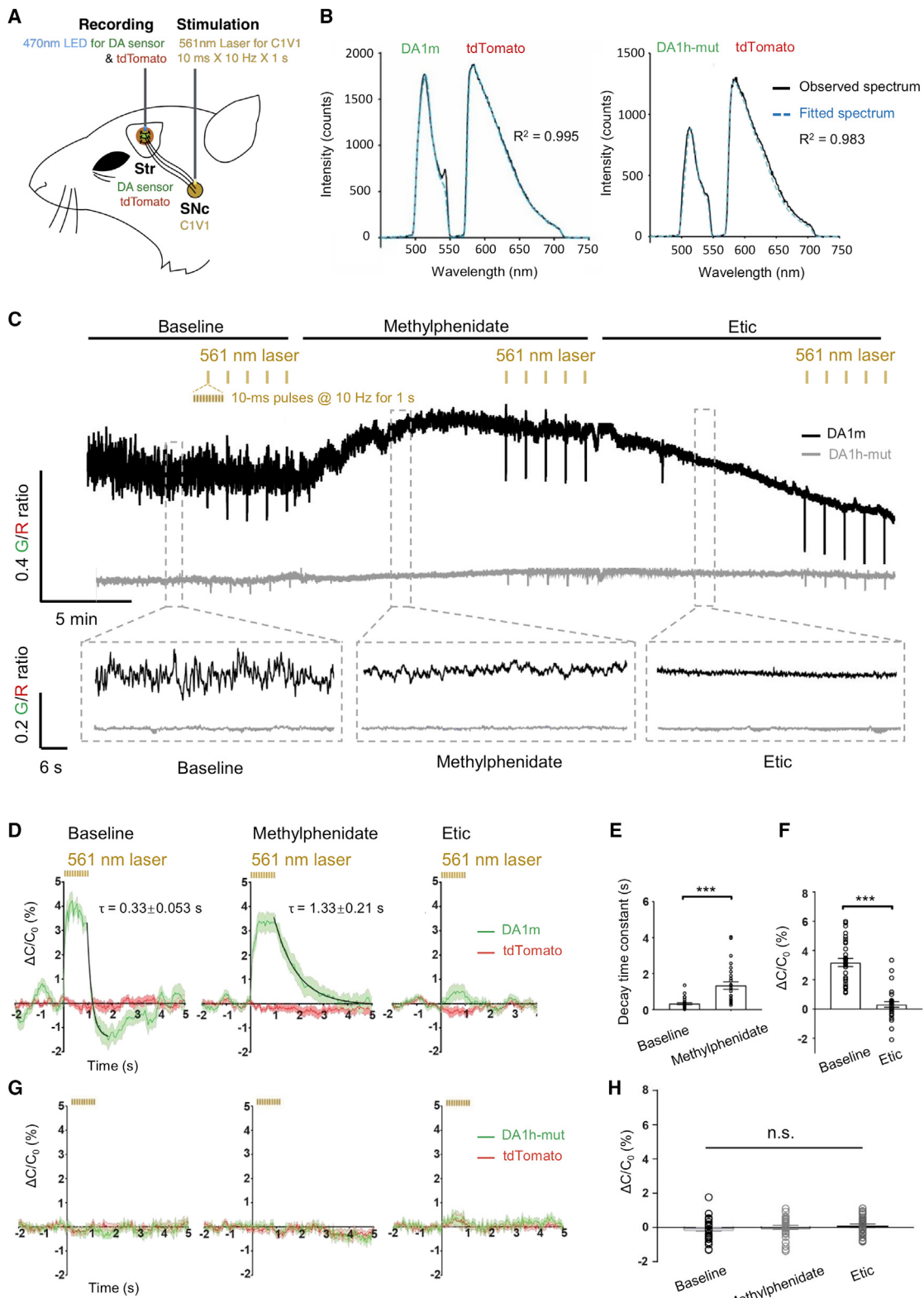


**Figure 5. Striatal DA Dynamics Measured in Freely Moving Mice during Optogenetic Stimulation of the SNC**

(A) Schematic depicting the dual-color optical recordings of DA1m-/DA1h-mut- and tdTomato-expressing neurons in the dorsal striatum during simultaneous optogenetic C1V1 stimulation of DANs in the SNC.

(legend continued on next page)

co-application of the antagonist Halo (Figures 4B–4D). In the tectal neuropil downstream of DANs, repeated application of capsaicin caused a progressive fluorescence increase that was also blocked by Halo (Figures 4E–4H). Presentation of a threatening looming stimulus elicited time-locked fluorescence increase specifically in the neuropil of tectal neurons, but not in their cell bodies (Figures 4I–4L). In summary, DA1m is well suited to report *in vivo* DA dynamics in the brain of zebrafish larvae.

### Combining Optogenetics with GRAB<sub>DA</sub> to Measure the Dynamics of DA in Freely Moving Mice

To test the ability of GRAB<sub>DA</sub> sensors to report DA dynamics in the mouse brain *in vivo*, we focused on DANs located in the substantia nigra pars compacta (SNc) that project to the dorsal striatum. We virally expressed DIO-C1V1 (Yizhar et al., 2011) in the SNc DANs of TH-Cre mice to permit their optogenetic activation. Co-expression of DA1m/DA1h-mut and tdTomato in the dorsal striatum allowed simultaneous monitoring of DA release and detection of movement-related artifacts (Figures 5A and 5B). In freely moving mice, the ratio of DA1m to tdTomato was elevated upon the administration of methylphenidate, a known DAT blocker (Volkow et al., 1999), and was suppressed by subsequent administration of Etic, a D<sub>2</sub>R blocker (Figure 5C). Transient fluctuations in the ratio are consistent with spontaneous DA release events during the animal movement (Balleine et al., 2007; da Silva et al., 2018; Howe and Dombeck, 2016). These transients were prolonged during methylphenidate application, and their amplitudes were reduced by Etic administration. In contrast, mice expressing the DA1h-mut did not show observable fluorescence changes (Figure 5C). Optogenetic activation of DANs in the SNc with C1V1 generated transient fluorescence increases in the dorsal striatum of DA1m-expressing mice, but not DA1h-mut-expressing mice (Figure 5D), which could also be prolonged by methylphenidate and abolished by Etic (Figures 5D–5H).

### Bi-directional Modulation of DA Dynamics in the NAc during Pavlovian Conditioning

In addition to the nigrostriatal pathway, the dopaminergic projection from the ventral tegmental area (VTA) to the NAc regulates a variety of important functions, including the reinforcement learning (Daw and Tobler, 2013; Glimcher, 2011; Gonzales et al., 2004). To test whether our sensors can detect behaviorally relevant changes in endogenous DA release, we first expressed DA1m or DA1h in the NAc of head-fixed, water-restricted mice

and trained them to associate a brief auditory cue with an ensuing reward (a drop of water), or a punishment (a brief air puff to the face) (Figure 6A). In every naive mouse, reward or punishment delivery triggered respective increases or decreases in the fluorescence signals in the NAc. Over the course of training, mice selectively learned to associate the reward-predictive cue with delivery of reward as the magnitude of the reward-evoked response decreased, while a response of a similar sign gradually developed to the reward-predictive cue (Figures 6B–6H). In summary, both DA1m and DA1h sensors have high signal-to-noise ratio and temporal resolution to report the dynamic bi-directional changes in DA release over the course of Pavlovian conditioning.

### Monitoring DA Release in the NAc of Mice during Male Mating Behaviors

In contrast to the well-established involvement of DA in Pavlovian conditioning, DA dynamics during naturally rewarding social behaviors (Berridge and Robinson, 1998), such as courtship and mating, remain largely a matter of debate. Here, we took advantage of the high sensitivity and fast temporal resolution of DA1h to better understand DA dynamics during sexual behaviors. To confirm that DA1h can detect acute DA release in the NAc, we virally expressed Cre-dependent Chrimson-tdTomato in the DANs in the VTA using DAT-ires-Cre mice. We observed that optogenetic stimulation evoked time-locked fluorescence increases of DA1h (Figures S6A–S6F). The DA1h signal peaked at the end of the 0.5-s stimulation and sharply decreased to pre-stimulation level by 2 s (Figures S6G and S6H).

During the behavioral test, a sexually receptive C57BL/6J female was introduced into the home cage of the male mouse, and the male quickly approached and investigated the female and initiated mounting within the first minute (Figures 7A and 7B). While sniffing the female, the fluorescence of DA1h measured in the male's NAc increased slightly in some animals. The fluorescence increases during mounting and intromission were highly reliable across all animals. During ejaculation, the fluorescence reached the largest response. Smaller but consistent fluorescence increases were also observed during penile grooming that typically occurred after intromission (Figures 7C and 7D). The average fluorescence increases during all behaviors except sniffing the female is significantly higher than values obtained from randomized controls (Figures 7E and 7F). In animals that expressed DA1h-mut in the NAc, we observed no significant increase of fluorescence during mounting,

(B) Representative frames of the emission spectra of DA1m/DA1h-mut and tdTomato co-expressed in the dorsal striatum. Black traces show the measured spectrum; the blue dashed traces show the fitting curves generated by a linear unmixing algorithm.

(C) Representative traces showing the ratio of DA1m (black) or DA1h-mut (gray) to tdTomato coefficients in a freely moving mouse (top panel) and enlarged traces (bottom panel) in the baseline (left) 5 min after the intraperitoneal (i.p.) injection of methylphenidate (10 mg/kg, middle), and 5 min after the i.p. injection of Etic (2 mg/kg, right). Black lines above indicate the time of compound administration. Yellow ticks indicate the time of optogenetic stimulation.

(D and G) Averaged fluorescence changes from DA1m/DA1h-mut (green) expressed in the dorsal striatum during optogenetic stimulation of DANs in the SNc by C1V1 under indicated conditions ( $n = 30$  trials from 6 hemispheres of 3 mice for each condition). Baseline (left), after the i.p. injection of methylphenidate (middle), and after the i.p. injection of Etic (right). The off kinetics were fitted with a single exponential function (black traces).  $\Delta C/C_0\%$  represents the percent change of the fluorescence coefficient of each fluorophore (see STAR Methods for details). Five data points (measured at 0.12 s, 0.32 s, 0.52 s, 0.72 s, and 0.92 s after the onset of the stimulation pulse train) were excluded to remove the stimulation artifacts.

(E) Comparison of the decay time constants of C1V1-evoked DA1m fluorescence responses between baseline group and methylphenidate group.

(F and H) Comparison of the magnitude of C1V1-evoked DA1m/DA1h-mut fluorescence changes between different groups.

Values with error bars indicate mean  $\pm$  SEM. Student's *t* test performed; n.s., not significant; \*\*\* $p < 0.001$ .

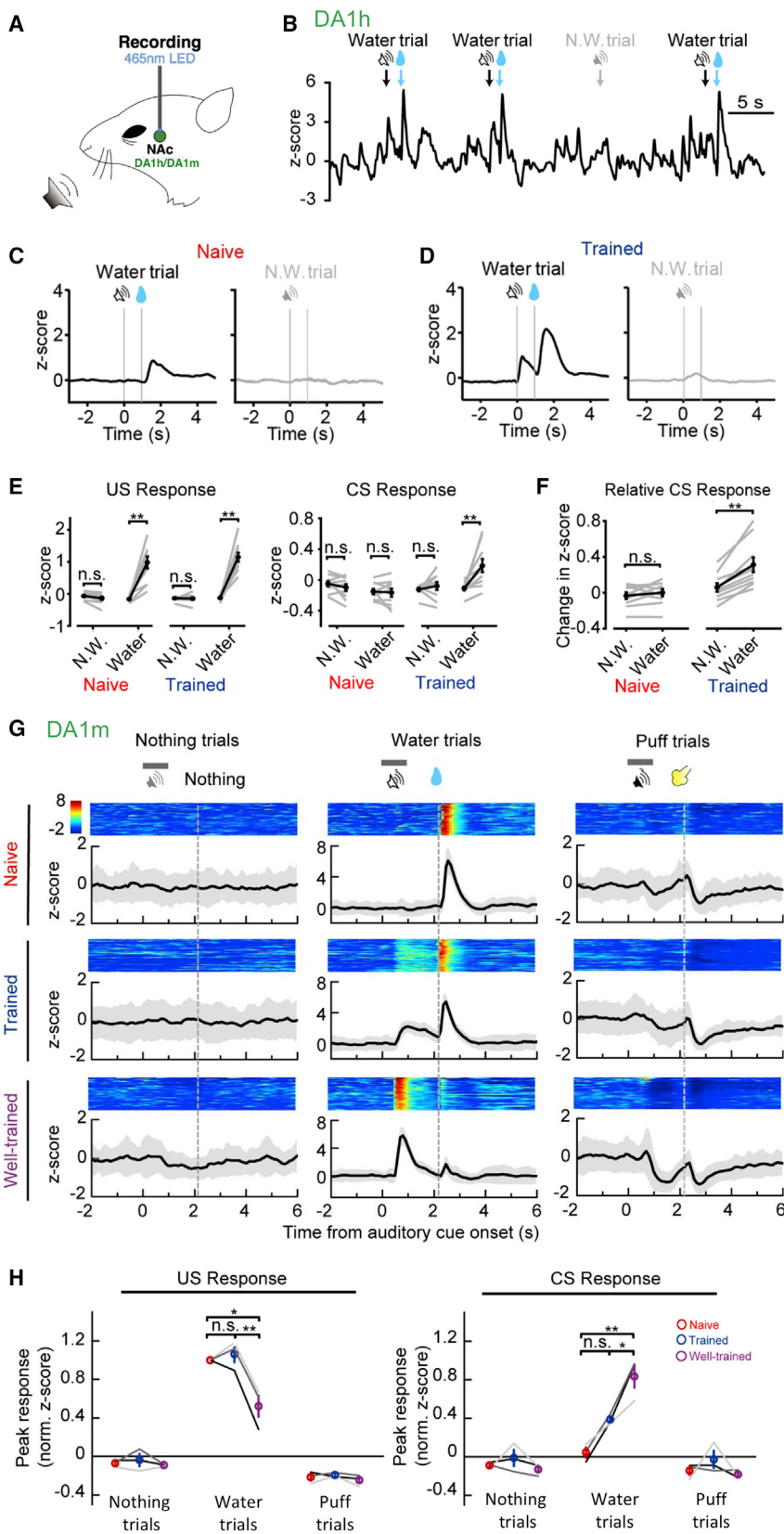


**Figure 6. DA Release in NAc Measured during Various Training Phases of an Auditory Pavlovian Conditioning Task**

(A) Schematic for fiber photometry recording of GRAB<sub>DA</sub>-expressing neurons from the NAc of a head-fixed mouse during auditory Pavlovian conditioning task.

(B) Exemplar trace of DA1h signals from a trained mouse encompassing four sequential trials. The timings of cues (CS) or water reward (US) are indicated above.

(C and D) Exemplar time-aligned DA1h signals from a mouse in naive (C) and trained (D) sessions. Note emergence of DA response to reward-predictive cue after training.

(E) Group analysis of DA1h responses to water (US, left) and cue (CS, right) of both naive and trained mice ( $n = 9$  mice; US response: naïve no water (N.W.):  $p = 0.084$ ; naïve water:  $p = 0.0020$ ; trained N.W.:  $p = 0.56$ ; trained water:  $p = 0.0020$ ; CS response: naïve N.W.:  $p = 0.37$ ; naïve water:  $p = 1.0000$ ; trained N.W.:  $p = 0.043$ ; trained water:  $p = 0.0020$ ).

(F) Direct comparison of baseline-subtracted DA1h signals to cue (CS) (naive:  $p = 0.43$ ; trained:  $p = 0.0020$ ).

(G) Exemplar time-aligned pseudocolor images and averaged traces (mean shaded with  $\pm$  SD) from a mouse in naive, trained, and well-trained sessions.

(H) Group analysis of the normalized peak Z scores of DA1m signals to US and CS in different sessions. Each trace (coded with specific gray value) represents data from one animal ( $n = 3$  mice; water trial US responses:  $p = 0.7638$  between naive and trained,  $p = 0.0125$  between naive and well-trained,  $p = 0.0080$  between trained and well-trained; water trial CS responses:  $p = 0.1032$  between naive and trained,  $p = 0.0067$  between naive and well-trained,  $p = 0.0471$  between trained and well-trained).

Values with error bars indicate mean  $\pm$  SEM. Signed rank test performed in (E) and (F); n.s., not significant; \*\* $p < 0.01$ . Post hoc Tukey's test was performed in (H); n.s., not significant; \* $p < 0.05$ ; \*\* $p < 0.01$ .

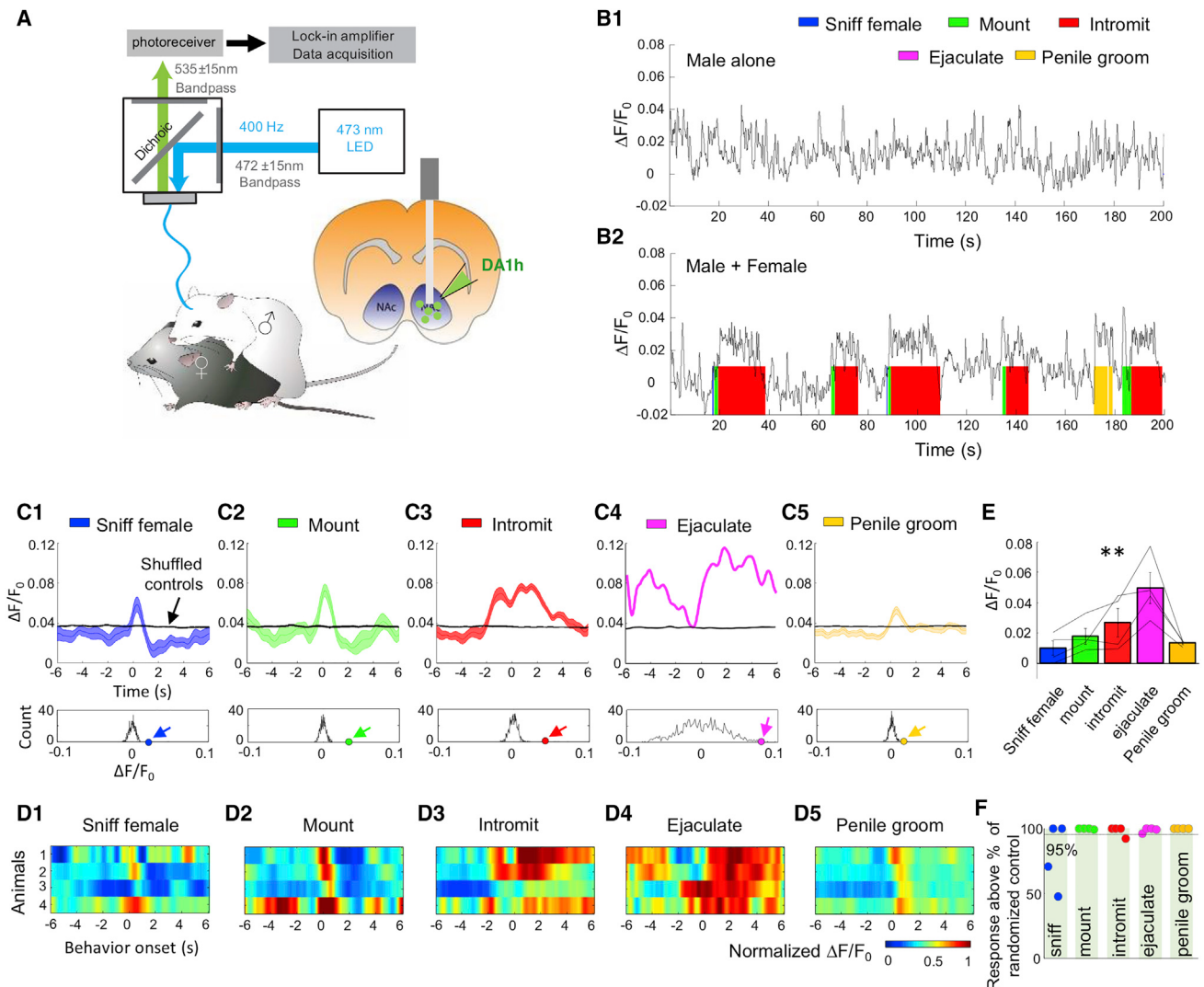


**Figure 7. Acute DA Release in the NAc Measured during Male Sexual Behaviors**

(A) Schematic depicting fiber photometry recording of DA1h-expressing neurons from the NAc of a male mouse during sexual behaviors.

(B1 and B2) Representative fluorescence changes before female introduction (B1) and during sexual behaviors (B2). The colored shades indicate different behavioral events.

(C1–C5) Top: representative post-event histograms (PETHs, mean shaded with  $\pm$  SEM) showing the DA1h signal aligned to onsets of various behavioral events from one mouse. Black lines show averaged PETHs of 1,000  $\times$  randomized controls. Bottom: the distributions of mean  $\Delta F/F_0$  of randomized controls. Colored dots and arrows indicate the actual mean  $\Delta F/F_0$  during the behaviors.

(D1–D5) Heatmap showing the PETHs of all four animals during various behaviors. For each animal,  $\Delta F/F_0$  is normalized with the maximum value during ejaculation.

(E) Group data summarizing the mean  $\Delta F/F_0$  during various behaviors of all four animals. Error bar:  $\pm$  SEM. One-way ANOVA with repeated measures. Among behaviors:  $F(3, 4) = 5.96$ ,  $p = 0.01$ .

(F) Each dot indicates the mean  $\Delta F/F_0$  value during one behavior of one animal in reference to the values of randomized controls. Most dots are at 100%, indicating that the mean  $\Delta F/F_0$  is higher than 100% of the 1,000  $\times$  shuffled controls.

See also Figure S6.

intromission, or ejaculation, suggesting that the DA1h fluorescence increases during sexual behaviors were not due to movement artifacts (Figure S6I–S6L). These results indicate that DA is acutely released in the NAc during episodes of sexual behaviors and could encode information about specific features of courtship and mating.

## DISCUSSION

Here, we describe the development and characterization of a pair of novel genetically encoded fluorescent sensors that enable specific, real-time detection of endogenous DA dynamics in several model systems *ex vivo* and *in vivo*. In acute mouse

brain slices, GRAB<sub>DA</sub> sensors reported stimulus-evoked DA release in mesolimbic pathway. In flies, GRAB<sub>DA</sub> sensors detected odor-evoked DA release in the MB and resolved DA release evoked by a single electrical stimulus. In transgenic zebrafish, GRAB<sub>DA</sub> sensors reported chemogenetically evoked and looming stimulation evoked DA release in the optic tectum. In mice, combining optogenetic stimulation with GRAB<sub>DA</sub> sensors enabled the simultaneous optical manipulation and detection of DA signals *in vivo*. Finally, GRAB<sub>DA</sub> sensors revealed real-time DA dynamics in the NAc of behaving mice during Pavlovian conditioning or sexual behaviors.

Our GRAB<sub>DA</sub> sensors exhibit several clear advantages over existing methods. First, GRAB<sub>DA</sub> sensors are genetically encoded by relatively small genes (~2 kb), making them amenable to transgenic approaches and viral packaging. Second, GRAB<sub>DA</sub> sensors have high sensitivity to DA. In response to DA, DA1m and DA1h sensors achieve a maximal  $\Delta F/F_0 \sim 90\%$  with ~130-nM and ~10-nM apparent affinities, respectively. In contrast, conventional GPCR-based fluorescence resonance energy transfer (FRET) probes for detecting neurotransmitters are usually limited to a maximum of ~5% under optimal conditions and less than that *in vivo* (Vilardaga et al., 2003; Ziegler et al., 2011). Third, GRAB<sub>DA</sub> sensors have high specificity for DA. Finally, GRAB<sub>DA</sub> sensors have rapid response kinetics with a rise time of  $\leq 100$  ms (Figures 2F, 3I, and S1). Although this response time of GRAB<sub>DA</sub> sensors is slower than FSCV, it is sufficiently rapid for reporting most physiologically relevant DA dynamics and shares response kinetics similar to WT GPCRs (Lohse et al., 2008). A recently described fluorescent DA sensor (named dLight) utilizes a similar detection strategy to report DA signaling *in vivo* (Patriarchi et al., 2018). The applied dLight variants report *in vivo* DA dynamics in rodent brains with similar kinetics and signal-to-noise ratio as GRAB<sub>DA</sub> sensors. However, the GRAB<sub>DA</sub> sensors have been optimized for brightness, have more consistent sensitivity ( $EC_{50}$ ) to DA across different cell types, and have proven efficacy in multiple organisms *in vivo*.

We note that the GRAB<sub>DA</sub> sensors have negligible coupling with major GPCR downstream pathways. This is presumably due to the steric hindrance imposed by the bulky cpEGFP moiety that replaces parts of the ICL3, which is the critical position for G protein or arrestin to interact with the GPCR (Luttrell and Lefkowitz, 2002; Neves et al., 2002). Consistent with minimal coupling between GRAB<sub>DA</sub> sensors and downstream signaling pathways, *in vivo* Ca<sup>2+</sup> imaging experiments using the Ca<sup>2+</sup> sensor jRCaMP1a revealed no measurable alteration in Ca<sup>2+</sup> signaling in neurons of transgenic flies that overexpressed GRAB<sub>DA</sub> sensors (Figures S5F–S5H).

Using GRAB<sub>DA</sub> sensors, we observed compartmentalized DA dynamics in the MB of flies, even down to single neuron level (Figure S5). Thus, GRAB<sub>DA</sub> sensors create new opportunities for exploring how specific compartments in the MB of the fly may exhibit distinct DA dynamics, which has been suggested by previous reports (Aso et al., 2014; Cognigni et al., 2018; Cohn et al., 2015; Mao and Davis, 2009). Experiments in flies also illustrate the power of GRAB<sub>DA</sub> sensors to probe DAT function *in vivo* by directly measuring extracellular DA levels in real time. GRAB<sub>DA</sub> sensors readily respond to visually induced DA release in the intact brain of the zebrafish larvae

as well, providing a robust and convenient tool to examine DA dynamics in this classic vertebrate model system.

Our experiments in behaving male mice provide new insight into the dynamics of DA during sexual behaviors. Contrary to previous reports revealed by either microdialysis or FSCV measurement, which described slow changes of extracellular DA during sexual behaviors (Pfau et al., 1990) or only transient increase during female introduction (Robinson et al., 2001), GRAB<sub>DA</sub> sensors revealed a time-locked DA elevation aligned to various sexual behaviors, consistent with a model where DA encodes behavioral motivation, anticipation, or arousal. As recent breakthroughs in single-cell sequencing have highlighted a previously unrecognized molecular, morphological, physiological, and functional heterogeneity of DANs (Nair-Roberts et al., 2008; Ungless and Grace, 2012), we expected that the targeted expression of genetically encoded GRAB<sub>DA</sub> sensors with cell-type specificity could therefore provide a critical window into the coding strategy of dopaminergic transmission in complex behaviors.

We anticipate that future efforts will be able to further tune the affinity, enhance the selectivity, and increase the signal-to-noise ratio of the next generation of GRAB<sub>DA</sub> sensors by using the recently solved crystal structure of the D<sub>2</sub>R (Wang et al., 2018). Moreover, by adding a red fluorescent protein, GRAB<sub>DA</sub> sensors can be readily transformed into ratiometric indicators, which could prove useful for more quantitative measurements of DA release across different experiments and preparations. Finally, a GPCR-based strategy was recently used to develop a genetically encoded sensor (GACh) with high sensitivity and high selectivity for acetylcholine (ACh) (Jing et al., 2018). Both sensors operate by coupling conformational changes in a GPCR induced by ligand binding to drive increases in cpEGFP fluorescence. Given the diverse ligand specificity of different GPCRs, a future goal will be to explore whether this principle can be expanded further to develop sensors for the entire range of known neurotransmitters and neuromodulators.

## STAR★METHODS

Detailed methods are provided in the online version of this paper and include the following:

- KEY RESOURCES TABLE
- CONTACT FOR REAGENT AND RESOURCE SHARING
- EXPERIMENTAL MODEL AND SUBJECT DETAILS
  - Primary cultures
  - Cell lines
  - Mice
  - Flies
  - Zebrafish
- METHOD DETAILS
  - Molecular biology
  - Expression of GRAB<sub>DA</sub> in cultured cells and *in vivo*
  - Fluorescence imaging of cultured cells
  - cAMP-dependent reporter gene assay
  - GTP-γ-S binding assay
  - Tango assay
  - Fluorescence imaging of GRAB<sub>DA</sub> in brain slices

- Fluorescence imaging of transgenic flies
- Fluorescence imaging of zebrafish
- Fiber Photometry recording in freely moving mice
- Behaviors

- QUANTIFICATION AND STATISTICAL ANALYSIS
- DATA AND SOFTWARE AVAILABILITY

#### SUPPLEMENTAL INFORMATION

Supplemental Information includes six figures, one table, and two videos and can be found with this article online at <https://doi.org/10.1016/j.cell.2018.06.042>.

#### ACKNOWLEDGMENTS

This work was supported by the National Basic Research Program of China (973 Program; grant 2015CB856402), the General Program of National Natural Science Foundation of China (project 31671118), the NIH BRAIN Initiative (NS103558), the Junior Thousand Talents Program of China, the grants from the Peking-Tsinghua Center for Life Sciences, and the State Key Laboratory of Membrane Biology at Peking University School of Life Sciences to Y. Li; the NIH training grants F32 NS083369 and K99 MH110597 to S.F.O.; the Junior Thousand Talents Program of China to S.Z.; the grant from the Ministry of Science and Technology of the People's Republic of China (2017YFA0505700) to M.X.; the Uehara postdoctoral fellowship to T.Y.; the NIH grants R01MH101377 and R21HD090563 and an Irma T. Hirsch Career Scientist Award to D.L.; and the Intramural Research Program of the NIH/NIEHS of the United States (1ZIAES103310) to G.C.

We thank Yi Rao for sharing the two-photon microscope and Xiaoguang Lei for the platform support of the Opera Phenix high-content screening system at PKU-CLS. We thank the Core Facilities at the School of Life Sciences, Peking University for technical assistance. We thank Richard Mooney, Yanhua Huang, and Liquan Luo for valuable feedback of the manuscript.

#### AUTHOR CONTRIBUTIONS

Y. Li conceived and supervised the project. F.S., M.J., and J. Zeng performed experiments related to sensor development, optimization, and characterization in culture HEK cells, culture neurons, brain slices, and transgenic flies, with help from H.W. and Z.Y., while the initial experiments were performed by Y. Luo and J.F. F.L. and J.D. designed and performed experiments on transgenic fish. J. Zhou, Y.G., T.Y., W.P., S.F.O., L.W., S.Z., D.L., M.X., A.C.K., and G.C. designed and performed experiments in behaving mice. All authors contributed to data interpretation and data analysis. Y. Li wrote the manuscript with input from F.S., J. Zeng, M.J., D.L., S.F.O., and M.X. and help from other authors.

#### DECLARATION OF INTERESTS

The authors declare competing financial interests. F.S., J. Zeng, M.J. and Y. Li have filed patent applications whose value might be affected by this publication.

Received: March 31, 2018  
 Revised: June 10, 2018  
 Accepted: June 22, 2018  
 Published: July 12, 2018

#### REFERENCES

- Allen, C., and Stevens, C.F. (1994). An evaluation of causes for unreliability of synaptic transmission. *Proc. Natl. Sci. USA* **91**, 10380–10383.
- Aso, Y., Hattori, D., Yu, Y., Johnston, R.M., Iyer, N.A., Ngo, T.T., Dionne, H., Abbott, L.F., Axel, R., Tanimoto, H., and Rubin, G.M. (2014). The neuronal architecture of the mushroom body provides a logic for associative learning. *eLife* **3**, e04577.
- Bainton, R.J., Tsai, L.T., Singh, C.M., Moore, M.S., Neckameyer, W.S., and Heberlein, U. (2000). Dopamine modulates acute responses to cocaine, nicotine and ethanol in *Drosophila*. *Curr. Biol.* **10**, 187–194.
- Balaji, J., and Ryan, T.A. (2007). Single-vesicle imaging reveals that synaptic vesicle exocytosis and endocytosis are coupled by a single stochastic mode. *Proc. Natl. Acad. Sci. USA* **104**, 20576–20581.
- Balleine, B.W., Delgado, M.R., and Hikosaka, O. (2007). The role of the dorsal striatum in reward and decision-making. *J. Neurosci.* **27**, 8161–8165.
- Barnea, G., Strapps, W., Herrada, G., Berman, Y., Ong, J., Kloss, B., Axel, R., and Lee, K.J. (2008). The genetic design of signaling cascades to record receptor activation. *Proc. Natl. Acad. Sci. USA* **105**, 64–69.
- Beaulieu, J.M., and Gainetdinov, R.R. (2011). The physiology, signaling, and pharmacology of dopamine receptors. *Pharmacol. Rev.* **63**, 182–217.
- Berridge, K.C., and Robinson, T.E. (1998). What is the role of dopamine in reward: hedonic impact, reward learning, or incentive salience? *Brain Res. Brain Res. Rev.* **28**, 309–369.
- Berry, J.A., Cervantes-Sandoval, I., Nicholas, E.P., and Davis, R.L. (2012). Dopamine is required for learning and forgetting in *Drosophila*. *Neuron* **74**, 530–542.
- Bungay, P.M., Newton-Vinson, P., Isele, W., Garris, P.A., and Justice, J.B. (2003). Microdialysis of dopamine interpreted with quantitative model incorporating probe implantation trauma. *J. Neurochem.* **86**, 932–946.
- Burke, C.J., Huetteroth, W., Owald, D., Perisse, E., Krashes, M.J., Das, G., Gohl, D., Silies, M., Certel, S., and Waddell, S. (2012). Layered reward signaling through octopamine and dopamine in *Drosophila*. *Nature* **492**, 433–437.
- Chefer, V.I., Thompson, A.C., Zapata, A., and Shippenberg, T.S. (2009). Overview of Brain Microdialysis. *Curr. Protoc. Neurosci.* **47**, 7.1.1–7.1.28.
- Cichewicz, K., Garren, E.J., Adiele, C., Aso, Y., Wang, Z., Wu, M., Birman, S., Rubin, G.M., and Hirsh, J. (2017). A new brain dopamine-deficient *Drosophila* and its pharmacological and genetic rescue. *Genes Brain Behav.* **16**, 394–403.
- Cognigni, P., Felsenberg, J., and Waddell, S. (2018). Do the right thing: neural network mechanisms of memory formation, expression and update in *Drosophila*. *Curr. Opin. Neurobiol.* **49**, 51–58.
- Cohn, R., Morantte, I., and Ruta, V. (2015). Coordinated and compartmentalized neuromodulation shapes sensory processing in *Drosophila*. *Cell* **163**, 1742–1755.
- Cook, E.H., Jr., Stein, M.A., Krasowski, M.D., Cox, N.J., Olkon, D.M., Kieffer, J.E., and Leventhal, B.L. (1995). Association of attention-deficit disorder and the dopamine transporter gene. *Am. J. Hum. Genet.* **56**, 993–998.
- da Silva, J.A., Tecuapetla, F., Paixão, V., and Costa, R.M. (2018). Dopamine neuron activity before action initiation gates and invigorates future movements. *Nature* **554**, 244–248.
- Dana, H., Mohar, B., Sun, Y., Narayan, S., Gordus, A., Hasseman, J.P., Tsegaye, G., Holt, G.T., Hu, A., Walpita, D., et al. (2016). Sensitive red protein calcium indicators for imaging neural activity. *eLife* **5**.
- Davis, R.L. (1993). Mushroom bodies and *Drosophila* learning. *Neuron* **11**, 1–14.
- Daw, N.D., and Tobler, P.N. (2013). Value Learning through Reinforcement: The Basics of Dopamine and Reinforcement Learning. In *Neuroeconomics*, P.W. Glimcher and E. Fehr, eds. (Elsevier), pp. 283–298.
- Di Chiara, G., and Imperato, A. (1988). Drugs abused by humans preferentially increase synaptic dopamine concentrations in the mesolimbic system of freely moving rats. *Proc. Natl. Acad. Sci. USA* **85**, 5274–5278.
- Florin-Lechner, S.M., Druhan, J.P., Aston-Jones, G., and Valentino, R.J. (1996). Enhanced norepinephrine release in prefrontal cortex with burst stimulation of the locus coeruleus. *Brain Res.* **742**, 89–97.
- Gibson, D.G., Young, L., Chuang, R.Y., Venter, J.C., Hutchison, C.A., 3rd, and Smith, H.O. (2009). Enzymatic assembly of DNA molecules up to several hundred kilobases. *Nat. Methods* **6**, 343–345.

- Glimcher, P.W. (2011). Understanding dopamine and reinforcement learning: the dopamine reward prediction error hypothesis. *Proc. Natl. Acad. Sci. USA* **108** (*Suppl 3*), 15647–15654.
- Gonzales, R.A., Job, M.O., and Doyon, W.M. (2004). The role of mesolimbic dopamine in the development and maintenance of ethanol reinforcement. *Pharmacol. Ther.* **103**, 121–146.
- Graybiel, A.M., Aosaki, T., Flaherty, A.W., and Kimura, M. (1994). The basal ganglia and adaptive motor control. *Science* **265**, 1826–1831.
- Heisenberg, M. (2003). Mushroom body memoir: from maps to models. *Nat. Rev. Neurosci.* **4**, 266–275.
- Holroyd, C.B., and Coles, M.G.H. (2002). The neural basis of human error processing: reinforcement learning, dopamine, and the error-related negativity. *Psychol. Rev.* **109**, 679–709.
- Howe, M.W., and Dombeck, D.A. (2016). Rapid signalling in distinct dopaminergic axons during locomotion and reward. *Nature* **535**, 505–510.
- Howes, O.D., and Kapur, S. (2009). The dopamine hypothesis of schizophrenia: version III—the final common pathway. *Schizophr. Bull.* **35**, 549–562.
- Hull, E.M., Meisel, R.M., and Sachs, B.D. (2002). Male Sexual Behavior. *Horm. Brain Behav.* **1**, 3–137.
- Inagaki, H.K., Ben-Tabou de-Leon, S., Wong, A.M., Jagadish, S., Ishimoto, H., Barnea, G., Kitamoto, T., Axel, R., and Anderson, D.J. (2012). Visualizing neuromodulation in vivo: TANGO-mapping of dopamine signaling reveals appetite control of sugar sensing. *Cell* **148**, 583–595.
- Jaqins-Gerstl, A., and Michael, A.C. (2015). A review of the effects of FSCV and microdialysis measurements on dopamine release in the surrounding tissue. *Analyst (Lond.)* **140**, 3696–3708.
- Jing, M., Zhang, P., Wang, G., Jiang, H., Mesik, L., Feng, J., Zeng, J., Wang, S., Looby, J., Guagliardo, N.A., et al. (2018). A genetically encoded fluorescent acetylcholine indicator. *Nat. Biotechnol.* **10**, 1038/nbt. 4184.
- Kim, M.W., Wang, W., Sanchez, M.I., Coukos, R., von Zastrow, M., and Ting, A.Y. (2017). Time-gated detection of protein-protein interactions with transcriptional readout. *eLife* **6**.
- Kimura, K., Ote, M., Tazawa, T., and Yamamoto, D. (2005). Fruitless specifies sexually dimorphic neural circuitry in the *Drosophila* brain. *Nature* **438**, 229–233.
- Kroeze, W.K., Sassano, M.F., Huang, X.P., Lansu, K., McCorry, J.D., Giguère, P.M., Sciaky, N., and Roth, B.L. (2015). PRESTO-Tango as an open-source resource for interrogation of the druggable human GPCRome. *Nat. Struct. Mol. Biol.* **22**, 362–369.
- Lee, D., Creed, M., Jung, K., Stefanelli, T., Wendler, D.J., Oh, W.C., Mignocchi, N.L., Lüscher, C., and Kwon, H.-B. (2017). Temporally precise labeling and control of neuromodulatory circuits in the mammalian brain. *Nat. Methods* **14**, 495–503.
- Liu, C., Plaçais, P.Y., Yamagata, N., Pfeiffer, B.D., Aso, Y., Friedrich, A.B., Siwanowicz, I., Rubin, G.M., Preat, T., and Tanimoto, H. (2012). A subset of dopamine neurons signals reward for odour memory in *Drosophila*. *Nature* **488**, 512–516.
- Lohse, M.J., Hein, P., Hoffmann, C., Nikolaev, V.O., Vilardaga, J.P., and Büemann, M. (2008). Kinetics of G-protein-coupled receptor signals in intact cells. *Br. J. Pharmacol.* **153** (*Suppl 1*), S125–S132.
- Lotharius, J., and Brundin, P. (2002). Pathogenesis of Parkinson's disease: dopamine, vesicles and  $\alpha$ -synuclein. *Nat. Rev. Neurosci.* **3**, 932–942.
- Luttrell, L.M., and Lefkowitz, R.J. (2002). The role of beta-arrestins in the termination and transduction of G-protein-coupled receptor signals. *J. Cell Sci.* **115**, 455–465.
- Mao, Z., and Davis, R.L. (2009). Eight different types of dopaminergic neurons innervate the *Drosophila* mushroom body neuropil: anatomical and physiological heterogeneity. *Front. Neural Circuits* **3**, 5.
- Meng, C., Zhou, J., Papaneri, A., Peddada, T., Xu, K., and Cui, G. (2018). Spectrally Resolved Fiber Photometry for Multi-component Analysis of Brain Circuits. *Neuron* **98**, 707–717.
- Miesenböck, G., De Angelis, D.A., and Rothman, J.E. (1998). Visualizing secretion and synaptic transmission with pH-sensitive green fluorescent proteins. *Nature* **394**, 192–195.
- Mintz, I.M., Sabatini, B.L., and Regehr, W.G. (1995). Calcium control of transmitter release at a cerebellar synapse. *Neuron* **15**, 675–688.
- Missale, C., Nash, S.R., Robinson, S.W., Jaber, M., and Caron, M.G. (1998). Dopamine receptors: from structure to function. *Physiol. Rev.* **78**, 189–225.
- Muller, A., Joseph, V., Slesinger, P.A., and Kleinfeld, D. (2014). Cell-based reporters reveal in vivo dynamics of dopamine and norepinephrine release in murine cortex. *Nat. Methods* **11**, 1245–1252.
- Nair-Roberts, R.G., Chatelain-Badic, S.D., Benson, E., White-Cooper, H., Bolam, J.P., and Ungless, M.A. (2008). Stereological estimates of dopaminergic, GABAergic and glutamatergic neurons in the ventral tegmental area, substantia nigra and retrorubral field in the rat. *Neuroscience* **152**, 1024–1031.
- Neves, S.R., Ram, P.T., and Iyengar, R. (2002). G protein pathways. *Science* **296**, 1636–1639.
- Ni, J.Q., Zhou, R., Czech, B., Liu, L.P., Holderbaum, L., Yang-Zhou, D., Shim, H.S., Tao, R., Handler, D., Karpowicz, P., et al. (2011). A genome-scale shRNA resource for transgenic RNAi in *Drosophila*. *Nat. Methods* **8**, 405–407.
- Nieoullon, A. (2002). Dopamine and the regulation of cognition and attention. *Prog. Neurobiol.* **67**, 53–83.
- Pacak, K., Palkovits, M., Kopin, I.J., and Goldstein, D.S. (1995). Stress-induced norepinephrine release in the hypothalamic paraventricular nucleus and pituitary-adrenocortical and sympathoadrenal activity: in vivo microdialysis studies. *Front. Neuroendocrinol.* **16**, 89–150.
- Patriarchi, T., Cho, J.R., Merten, K., Howe, M.W., Marley, A., Xiong, W.H., Folk, R.W., Broussard, G.J., Liang, R., Jang, M.J., et al. (2018). Ultrafast neuronal imaging of dopamine dynamics with designed genetically encoded sensors. *Science*. Published online May 31, 2018. <https://doi.org/10.1126/science.aat4422>.
- Pfaus, J.G., Damsma, G., Nomikos, G.G., Wenkstern, D.G., Blaha, C.D., Phillips, A.G., and Fibiger, H.C. (1990). Sexual behavior enhances central dopamine transmission in the male rat. *Brain Res.* **530**, 345–348.
- Pfeiffer, B.D., Truman, J.W., and Rubin, G.M. (2012). Using translational enhancers to increase transgene expression in *Drosophila*. *Proc. Natl. Acad. Sci. USA* **109**, 6626–6631.
- Ritz, M.C., Lamb, R.J., Goldberg, S.R., and Kuhar, M.J. (1987). Cocaine receptors on dopamine transporters are related to self-administration of cocaine. *Science* **237**, 1219–1223.
- Robinson, D.L., Phillips, P.E.M., Budygin, E.A., Trafton, B.J., Garris, P.A., and Wightman, R.M. (2001). Sub-second changes in accumbal dopamine during sexual behavior in male rats. *Neuroreport* **12**, 2549–2552.
- Robinson, D.L., Venton, B.J., Heien, M.L., and Wightman, R.M. (2003). Detecting subsecond dopamine release with fast-scan cyclic voltammetry in vivo. *Clin. Chem.* **49**, 1763–1773.
- Robinson, D.L., Hermans, A., Seipel, A.T., and Wightman, R.M. (2008). Monitoring rapid chemical communication in the brain. *Chem. Rev.* **108**, 2554–2584.
- Schultz, W. (2007). Behavioral dopamine signals. *Trends Neurosci.* **30**, 203–210.
- Schultz, W. (2016). Dopamine reward prediction-error signalling: a two-component response. *Nat. Rev. Neurosci.* **17**, 183–195.
- Schwaerzel, M., Monastirioti, M., Scholz, H., Friggi-Grelin, F., Birman, S., and Heisenberg, M. (2003). Dopamine and octopamine differentiate between aversive and appetitive olfactory memories in *Drosophila*. *J. Neurosci.* **23**, 10495–10502.
- Singleman, C., and Holtzman, N.G. (2014). Growth and maturation in the zebrafish, *Danio rerio*: a staging tool for teaching and research. *Zebrafish* **11**, 396–406.
- Smith, A.D., Olson, R.J., and Justice, J.B., Jr. (1992). Quantitative microdialysis of dopamine in the striatum: effect of circadian variation. *J. Neurosci. Methods* **44**, 33–41.

- Sokoloff, P., Giros, B., Martres, M.-P., Bouthenet, M.-L., and Schwartz, J.-C. (1990). Molecular cloning and characterization of a novel dopamine receptor (D3) as a target for neuroleptics. *Nature* 347, 146–151.
- Tanaka, N.K., Tanimoto, H., and Ito, K. (2008). Neuronal assemblies of the *Drosophila* mushroom body. *J. Comp. Neurol.* 508, 711–755.
- Tidey, J.W., and Miczek, K.A. (1996). Social defeat stress selectively alters mesocorticolimbic dopamine release: an *in vivo* microdialysis study. *Brain Res.* 721, 140–149.
- Ungless, M.A., and Grace, A.A. (2012). Are you or aren't you? Challenges associated with physiologically identifying dopamine neurons. *Trends Neurosci.* 35, 422–430.
- Villardaga, J.-P., Büinemann, M., Krasel, C., Castro, M., and Lohse, M.J. (2003). Measurement of the millisecond activation switch of G protein-coupled receptors in living cells. *Nat. Biotechnol.* 21, 807–812.
- Volkow, N.D., Wang, G.J., Fowler, J.S., Fischman, M., Foltin, R., Abumrad, N.N., Gatley, S.J., Logan, J., Wong, C., Gifford, A., et al. (1999). Methylphenidate and cocaine have a similar *in vivo* potency to block dopamine transporters in the human brain. *Life Sci.* 65, PL7–PL12.
- Wang, S., Che, T., Levit, A., Shoichet, B.K., Wacker, D., and Roth, B.L. (2018). Structure of the D2 dopamine receptor bound to the atypical antipsychotic drug risperidone. *Nature* 555, 269–273.
- Wise, R.A. (2004). Dopamine, learning and motivation. *Nat. Rev. Neurosci.* 5, 483–494.
- Wu, M.V., and Shah, N.M. (2011). Control of masculinization of the brain and behavior. *Curr. Opin. Neurobiol.* 21, 116–123.
- Yizhar, O., Fenno, L.E., Prigge, M., Schneider, F., Davidson, T.J., O'Shea, D.J., Sohal, V.S., Goshen, I., Finkelstein, J., Paz, J.T., et al. (2011). Neocortical excitation/inhibition balance in information processing and social dysfunction. *Nature* 477, 171–178.
- Yusa, K., Zhou, L., Li, M.A., Bradley, A., and Craig, N.L. (2011). A hyperactive piggyBac transposase for mammalian applications. *Proc. Natl. Acad. Sci. USA* 108, 1531–1536.
- Ziegler, N., Bätz, J., Zabel, U., Lohse, M.J., and Hoffmann, C. (2011). FRET-based sensors for the human M1-, M3-, and M5-acetylcholine receptors. *Bioorg. Med. Chem.* 19, 1048–1054.

**STAR★METHODS****KEY RESOURCES TABLE**

REAGENT or RESOURCE	SOURCE	IDENTIFIER
<b>Antibodies</b>		
Chicken polyclonal anti-GFP antibody	Abcam	Cat#ab13970; RRID:AB_300798
Rabbit polyclonal anti-tyrosine hydroxylase (TH) antibody	Millipore	Cat#ab152; RRID:AB_390204
Alexa 488-conjugated goat-anti-chicken IgG (H+L)	Invitrogen	Cat#A11039
Alexa-555-conjugated goat-anti-rabbit IgG (H+L)	AAT-Bio	Cat#16690
<b>Bacterial and Virus Strains</b>		
AAV-hSyn-DA1m	Vigene Biosciences	N/A
AAV-hSyn-DA1h	Vigene Biosciences	N/A
AAV-Ef1a-DIO-C1V1-YFP	NIEHS Viral Vector Core	N/A
AAV-hSyn-DA1m-mut	Vigene Biosciences	N/A
AAV-hSyn-DA1h-mut	Vigene Biosciences	N/A
AAV-hSyn-tdTomato	NIEHS Viral Vector Core	N/A
AAV-hSyn-Flex-ChrimsonR-tdTomato	UNC Vector Core	N/A
<b>Chemicals, Peptides, and Recombinant Proteins</b>		
Dopamine hydrochloride (DA)	Sigma-Aldrich	Cat#H8502
Haloperidol hydrochloride (Halo)	Tocris	Cat#0931
SCH 23390 hydrochloride (SCH)	Tocris	Cat#0925
Eticlopride hydrochloride (Etic)	Tocris	Cat#1847
L-DOPA	Abcam	Cat#ab120573
Serotonin hydrochloride (5-HT)	Tocris	Cat#3547
Histamine dihydrochloride (His)	Tocris	Cat#3545
L-Glutamic acid (Glu)	Sigma-Aldrich	Cat#V900408
GABA	Tocris	Cat#0344
Adenosine (Ado)	Tocris	Cat#3624
Acetylcholine chloride (ACh)	Solarbio	Cat#G8320
Tyramine (Tyr)	Sigma-Aldrich	Cat#V900670
Octopamine hydrochloride (Oct)	Tocris	Cat#2242
Noradrenaline bitartrate (NE)	Tocris	Cat#5169
Cocaine hydrochloride	Qinghai Pharmaceuticals	N/A
(E)-Capsaicin	Tocris	Cat#0462
<i>Threo</i> -methylphenidate hydrochloride	Tocris	Cat#1812
GTP- $\gamma$ -S	Sigma-Aldrich	Cat#10220647001
Digitonin	Sigma-Aldrich	Cat#D141
Isoamyl acetate	Sigma-Aldrich	Cat#306967
2,2,2-Tribromoethanol (Avetin)	Sigma-Aldrich	Cat#T48402
Isoflurane	RWD Life Science	Cat#R510-22
Forskolin	Sigma-Aldrich	Cat#F6886
$\alpha$ -bungarotoxin	Tocris	Cat#2133
Low melting-point agarose	Sigma-Aldrich	Cat#A9414
T5-exonuclease	New England Biolabs	Cat#M0363S
Phusion DNA polymerase	Thermo Fisher Scientific	Cat#F530L
Taq ligase	iCloning	Cat#TDL-100

(Continued on next page)

**Continued**

REAGENT or RESOURCE	SOURCE	IDENTIFIER
Critical Commercial Assays		
NanoLuc Luciferase Assay	Promega	Cat#N1110
Experimental Models: Cell Lines		
HEK293T	ATCC	Cat#CRL-3216; RRID:CVCL_0063
HeLa	ATCC	Cat#CCL-2; RRID:CVCL_0030
Luciferase reporter cell line for tango assay (Kroeze et al., 2015)	Gift from Bryan L Roth	N/A
HEK293T cell line stably expressing DA1h	This paper	N/A
HEK293T cell line stably expressing D <sub>2</sub> R	This paper	N/A
Experimental Models: Organisms/Strains		
Mouse: wild-type Sprague-Dawley rat pups (P0)	Beijing Vital River Laboratory Animal Technology	<a href="http://www.vitalriver.com/">http://www.vitalriver.com/</a>
Mouse: wild-type C57BL/6	Beijing Vital River Laboratory Animal Technology/Charles River Laboratories	<a href="http://www.vitalriver.com/">http://www.vitalriver.com/</a> <a href="https://www.criver.com/">https://www.criver.com/</a>
Mouse: B6.FVB(Cg)-Tg(Th-cre)Fl172Gsat/Mmucd	MMRRC	RRID:MMRRC_031029-UCD
Mouse: DAT-IRES-Cre	Jackson Laboratory	Stock#006660
Zebrafish: albino (slc45a2 <sup>b4</sup> ) (The background strain)	ZFIN	N/A
Zebrafish: Tg (elval3: DA1m)	This paper	N/A
Zebrafish: Tg (DAT:TRPV1-TagRFP) Tg; (elval3: DA1m)	This paper	N/A
<i>D. melanogaster</i> : UAS-DA1m/cyo (The line carrying DA1m on the chromosome 2)	This paper	N/A
<i>D. melanogaster</i> : UAS-DA1m/TM2 (The line carrying DA1m on the chromosome 3)	This paper	N/A
<i>D. melanogaster</i> : TH-GAL4	Gift from Yi Rao	Unpublished
<i>D. melanogaster</i> : C305a-GAL4	Gift from Yi Rao	BDSC: 30829
<i>D. melanogaster</i> : 30y-GAL4	Gift from Yi Rao	BDSC: 30818
<i>D. melanogaster</i> : DTH <sup>FS+/-</sup> ple <sup>2</sup> /TM6B (Cichewicz et al., 2017)	Gift from Jay Hirsh	N/A
<i>D. melanogaster</i> : UAS-DAT-RNAi (Ni et al., 2011)	Tsinghua Fly center	Tsinghua Fly center: TH01470.N
<i>D. melanogaster</i> : UAS-jRCaMP1a (Dana et al., 2016)	Gift from Chuan Zhou	BDSC: 63792
<i>D. melanogaster</i> : MB296B-GAL4 (Aso et al., 2014)	Gift from Hongtao Qin	Fly Light Split-GAL4 Driver Collection: 2135344
Oligonucleotides		
PCR primers	This paper	See Table S1
Recombinant DNA		
pDisplay vector	Invitrogen	Cat#V66020
pDisplay-DA1m-IRES-mCherry-CAAX	This paper	N/A
pDisplay-DA1h-IRES-mCherry-CAAX	This paper	N/A
pDisplay-DA1m-mut-IRES-mCherry-CAAX	This paper	N/A
pDisplay-DA1h-mut-IRES-mCherry-CAAX	This paper	N/A
pAAV-TRE-DA1m	This paper	N/A
pAAV-TRE-DA1m-mut	This paper	N/A
pAAV-hSyn-DA1m	This paper	Addgene: 113049
pAAV-hSyn-DA1h	This paper	Addgene: 113050
pAAV-hSyn-DA1h-mut	This paper	N/A

(Continued on next page)

***Continued***

REAGENT or RESOURCE	SOURCE	IDENTIFIER
Full-length human GPCR cDNAs	human ORFeome 8.1	<a href="http://horfdb.dfci.harvard.edu/">http://horfdb.dfci.harvard.edu/</a>
pDisplay-D <sub>2</sub> R-EGFP(ICL3)-IRES-mCherry-CAAX	This paper	N/A
pDisplay-D <sub>1</sub> R-cpEGFP(ICL3)-IRES-mCherry-CAAX	This paper	N/A
pDisplay-D <sub>2</sub> R-cpEGFP(ICL3)-IRES-mCherry-CAAX	This paper	N/A
pDisplay-D <sub>3</sub> R-cpEGFP(ICL3)-IRES-mCherry-CAAX	This paper	N/A
pDisplay-D <sub>4</sub> R-cpEGFP(ICL3)-IRES-mCherry-CAAX	This paper	N/A
pDisplay-D <sub>5</sub> R-cpEGFP(ICL3)-IRES-mCherry-CAAX	This paper	N/A
pDisplay-pHluorin-D <sub>2</sub> R	This paper	N/A
mScarlet-CAAX-N3	This paper	N/A
EGFP-CAAX-N3	This paper	N/A
KDELR1-EGFP-N3	This paper	N/A
PSD95-mScarlet-N3	This paper	N/A
Synaptophysin-mScarlet-N3	This paper	N/A
pPacific-D <sub>2</sub> R (for cell line construction)	This paper	N/A
pPacific-DA1h (for cell line construction)	This paper	N/A
pCS7-PiggyBAC	VIEWSOLID BIOTECH	N/A
pCS7-PiggyBAC (S103P, S509G) (Yusa et al., 2011)	This paper	N/A
pUAST	Gift from Yi Rao	N/A
pUAST-DA1m	This paper	N/A
pJFRC28	(Pfeiffer et al., 2012)	Addgene: 36431
pJFRC28-DA1m-mut	This paper	N/A
pTol2-elval3: DA1m	This paper	N/A
Tol2 mRNA	This paper	N/A
Software and Algorithms		
ImageJ	NIH	<a href="https://imagej.nih.gov/ij/">https://imagej.nih.gov/ij/</a> ; RRID:SCR_003070
Origin 9.1	OriginLab	<a href="https://www.originlab.com/">https://www.originlab.com/</a>
MATLAB	MathWorks	<a href="https://www.mathworks.com/products/matlab.html">https://www.mathworks.com/products/matlab.html</a> ; RRID:SCR_001622
Arduino	Arduino	<a href="https://www.arduino.cc">https://www.arduino.cc</a>
Linear Spectral Unmixing Algorithm v1.1	NIH	<a href="https://www.niehs.nih.gov/research/atniehs/labs/ln/pi/iv/tools/index.cfm">https://www.niehs.nih.gov/research/atniehs/labs/ln/pi/iv/tools/index.cfm</a>
Other		
Microsyringe pumps for virus injection	WPI/ Drummond Scientific	Nanoliter 2000 Injector/ Nanoject II
Inverted confocal microscope	Nikon	Ti-E A1
Inverted confocal microscope	Olympus	FV3000
Upright confocal microscope	Olympus	FV1000
Opera Phenix high content screening system	PerkinElmer	Cat#HH14000000
Multilabel plate reader	PerkinElmer	VICTOR X5
Vibratome	Leica	VT1200
Cryostat	Leica	CM1900
Two-photon microscope	Olympus	FV1000MPE
Mai Tai Ti:Sapphire laser	Spectra-Physics	Deepsee
Optical fibers	Thorlabs	FT200UMT/FT400UMT/BFH48-400
Implanted ferrule	Thorlabs	SF440-10
Blue LED light	Thorlabs	M470F1
Blue LED driver	Thorlabs	LEDD1B
Femtowatt Silicon Photoreceiver	Newport	2151
BioAmp processor	TDT	RZ5/RZ2

## CONTACT FOR REAGENT AND RESOURCE SHARING

Further information and requests for resources and reagents should be directed to and will be fulfilled by the Lead Contact, Yulong Li ([Yulongli@pku.edu.cn](mailto:Yulongli@pku.edu.cn)).

## EXPERIMENTAL MODEL AND SUBJECT DETAILS

### Primary cultures

Rat cortical neurons were prepared from postnatal 0-day old (P0) Sprague-Dawley rat pups (male and female, random choice; Beijing Vital River). The cortical neurons were dissociated from the dissected rat brains in 0.25% Trypsin-EDTA (GIBCO), and plated on 12-mm glass coverslips coated with poly-D-lysine (Sigma-Aldrich) in neurobasal medium (GIBCO) containing 2% B-27 supplement (GIBCO), 1% GlutaMax (GIBCO), and 1% penicillin-streptomycin (GIBCO). The neurons were cultured at 37°C in 5% CO<sub>2</sub>.

### Cell lines

HEK293T cell line (female, ATCC, CRL-3216) and HeLa cell line (female, ATCC, CCL-2) were bought from ATCC and authenticated based on the morphology under microscope and the analysis of the growth curve. HEK293T cell lines stably expressing D<sub>2</sub>R or DA1h were established in our laboratory. In brief, pPacific-D<sub>2</sub>R and pPacific-DA1h were constructed (pPacific was a self-constructed vector containing elements including 3' TR, DNA encoding myc tag, 2A sequence, DNA encoding mcherry, DNA encoding puromycin and 5' TR), and transfected with pCS7-PiggyBAC (S103P, S509G) ([Yusa et al., 2011](#)) into HEK293T cells, then the transfected cells were selected with 1 µg/ml puromycin. HEK293 cell line (female) stably expressing a tTA-dependent luciferase reporter and a β-arrestin2-TEV fusion construct was a gift from Bryan L Roth ([Kroeze et al., 2015](#)). Cell lines were cultured in DMEM (GIBCO) supplemented with 10% (v/v) FBS (GIBCO) and 1% penicillin-streptomycin (GIBCO) at 37°C in 5% CO<sub>2</sub>.

### Mice

P28–48 wild-type C57BL/6, TH-Cre mice and DAT-IRES-Cre mice were used to prepare the acute brain slices and *in vivo* fiber photometry experiments. Except in sexual behavior experiments the optical fibers were implanted on male mice, in other experiments fiber photometry recordings were performed in both male and female mice randomly, as the dopaminergic innervations mentioned in this paper are similar between them ([Wu and Shah, 2011](#)). All animals were maintained in the animal facilities and were family- or pair-housed in a temperature-controlled room with a 12-h/12-h light/dark cycle. All procedures for animal surgery and maintenance were performed using protocols that were approved by the Animal Care & Use Committees at Peking University, Chinese Academy of Sciences (CAS), New York University, University of California, San Francisco, and US National Institutes of Health, and were performed in accordance with the guidelines established by US National Institutes of Health guidelines.

### Flies

To generate transgenic flies, the coding sequence of DA1m was integrated into the pUAST vector using Gibson Assembly ([Gibson et al., 2009](#)), which was then used in P-element-mediated random insertion. Transgenic *Drosophila* lines carrying DA1m on the chromosomes 2 (UAS-DA1m/cyo) and 3 (UAS-DA1m/TM2) with the strongest expression level after crossing with TH-GAL4 were used. The coding sequence of DA1m-mut was incorporated into pJFRC28 ([Pfeiffer et al., 2012](#)) (Addgene plasmid #36431) using Gibson Assembly, and this plasmid was used to generate transgenic flies using PhiC31-mediated site-directed integration into attP40. The embryo injections were performed at Core Facility of *Drosophila* Resource and Technology, Shanghai Institute of Biochemistry and Cell Biology, CAS. Transgenic flies were raised on conventional corn meal at 25°C, with ~70% humidity, under 12-h/12-h light/dark cycle.

The fly lines used in this study: TH-GAL4, a gift and unpublished line generated by appending 2A-GAL4 to the last exon of TH, from Yi Rao, Peking University. C305a-GAL4 (BDSC: 30829) and 30y-GAL4 (BDSC: 30818), also gifts from Yi Rao. DTH<sup>FS+/-ple<sup>2</sup>/TM6B</sup> ([Cichewicz et al., 2017](#)), a gift from Jay Hirsh, University of Virginia. UAS-DAT-RNAi (TH01470.N) ([Ni et al., 2011](#)), from Tsinghua Fly center, Tsinghua University. UAS-jRCaMP1a (BDSC: 63792) ([Dana et al., 2016](#)), a gift from Chuan Zhou, Institute of Zoology, Chinese Academy of Sciences. MB296B-GAL4 ([Aso et al., 2014](#)), a gift from Hongtao Qin, Hunan University.

Adult *Drosophila* within 3 weeks after eclosion were used for imaging experiments. Both male and female were randomly used because dopaminergic projections to the MB are similar between them ([Kimura et al., 2005](#)). The flies corresponding to figures:

#### Figures 3A–3C

UAS-DA1m/cyo; TH-GAL4 (DANs)/TM6B

UAS-DA1m-mut/+; TH-GAL4/+

C305a-GAL4 (α' and β' Kenyon cells)/UAS-DA1m; DTH<sup>FS+/-ple<sup>2</sup>/+</sup> (WT group)

C305a-GAL4/UAS-DA1m; DTH<sup>FS+/-ple<sup>2</sup></sup> (TH-deficient group)

#### Figures 3D–3K

UAS-DA1m/cyo; TH-GAL4/TM6

UAS-DA1m-mut/+; TH-GAL4/+

**Figures 3L–3O**

UAS-DA1m/cyo; TH-GAL4/TM6B  
UAS-DA1m/+; TH-GAL4/UAS-DAT-RNAi

**Figures S5A and S5B**

UAS-DA1m/cyo; TH-GAL4/TM6B  
Fig.S5C-E  
MB296B-GAL4 > UAS-DA1m  
Fig.S5F-H  
TH-GAL4/ UAS-jRCaMP1a  
UAS-DA1m/+; TH-GAL4/UAS-jRCaMP1a  
30y-GAL4/ UAS-jRCaMP1a  
UAS-DA1m/+; 30y-GAL4/UAS-jRCaMP1a

**Zebrafish**

The background strain is albino (*slc45a2<sup>b4</sup>*). To generate transgenic zebrafish, plasmids containing pTol2-elval3: DA1m (25 ng/μL) and Tol2 mRNA (25 ng/μL) were co-injected into fertilized eggs, and founders were screened three months later. Transgenic zebrafish adults and larvae were maintained at 28°C on a 14-h/10-h light/dark cycle. Experiments were performed on 5 days-post-fertilization (dpf) larvae. Larval zebrafish do not have sex differentiation before 1-month post fertilization (Singleman and Holtzman, 2014).

**METHOD DETAILS****Molecular biology**

Plasmids were generated using Gibson Assembly. DNA fragments were generated using PCR amplification with primers (Thermo Fisher Scientific) with 30-bp overlap. The fragments were assembled using T5-exonuclease (New England Biolabs), Phusion DNA polymerase (Thermo Fisher Scientific), and Taq ligase (iCloning). All sequences were verified using Sanger sequencing (Sequencing platform in the School of Life Sciences of Peking University). DNA encoding the various DA receptor subtypes (D<sub>1</sub>R-D<sub>5</sub>R) was generated using PCR amplification of the full-length human GPCR cDNAs (hORFeome database 8.1). For characterization in HEK293T cells, the GRAB<sub>DA</sub> constructs were cloned into the pDisplay vector (Invitrogen), with an IgK leader sequence inserted upstream of the coding region. The IRES-mCherry-CAAX gene was attached downstream of GRAB<sub>DA</sub> and was used as a reference of membrane marker to calibrate the signal intensity. Site-directed mutagenesis of the N- and C-terminal linker sequences in cpEGFP was performed using primers containing randomized NNB codons (48 codons in total, encoding the 20 possible amino acids; Thermo Fisher Scientific). Site-directed mutagenesis of the D<sub>2</sub>R gene was performed using primers containing the target sites. For characterization in cultured neurons, the GRAB<sub>DA</sub> constructs were cloned into the pAAV vector under the TRE promoter or the human synapsin promoter. The marker constructs RFP(mScarlet)-CAAX, EGFP-CAAX, KDELR1-EGFP, PSD95- RFP(mScarlet) and synaptophysin-RFP(mScarlet) were cloned into pEGFP-N3 vector. To assess the brightness of GRAB<sub>DA</sub> sensors, D<sub>2</sub>R-EGFP chimera with EGFP inserted into the same insertion site within ICL3 was constructed as the reference. The pH sensitive fluorescent protein pHluorin (Miesenböck et al., 1998) was attached to the N terminus of D<sub>2</sub>R to measure the internalization of D<sub>2</sub>R in response to DA application. To generate stable cell lines expressing D<sub>2</sub>R or DA1h, a self-constructed vector containing elements including 3' TR, DNA encoding myc tag, 2A sequence, DNA encoding mcherry, DNA encoding puromycin and 5' TR was made. The DNA of D<sub>2</sub>R or DA1h was cloned into the pPacific vector using Gibson Assembly. Two mutations (S103P and S509G) were introduced to pCS7-PiggyBAC (VIEWSOLID BIOTECH) to generate a hyperactive piggyBac transposase (Yusa et al., 2011) for the construction of stable cell lines.

**Expression of GRAB<sub>DA</sub> in cultured cells and *in vivo***

The HEK293T cells and HeLa cells were plated on 12-mm glass coverslips in 24-well plates and grown to ~50% confluence for transfection. Transfection was performed by incubating the cells with a mixture containing 1-μg DNA and 3-μg PEI for 6 h. Imaging was performed 24–48 h after transfection.

The cultured neurons were transfected 7–9 days later using the calcium phosphate transfection method. Transfection was performed by incubating the neurons with a mixture containing 125mM CaCl<sub>2</sub>, HBS (pH 7.04–7.12) and 2 μg DNA for 2 h. Then the DNA-Ca<sub>3</sub>(PO<sub>4</sub>)<sub>2</sub> precipitate was removed from the culture by washing the coverslips with preheated HBS (pH 6.80). Imaging was performed 48–72 h after transfection.

For *in vivo* expression, mice with the age of P42–60 were first anesthetized by 2,2,2-Tribromoethanol (Avetin, 500 mg/kg, Sigma-Aldrich) through intraperitoneal injection, or by isoflurane (RWD Life Science), and then placed in a stereotaxic frame to inject AAVs with a microsyringe pump (Nanoliter 2000 Injector, WPI, or Nanoject II, Drummond Scientific). In Figure 5, the AAVs of hSyn-DA1m/DA1h-mut and hSyn-tdTomato were injected in the dorsal striatum (AP: -0.5mm, ML: ± 2.5mm, and DV: -2.2mm), and the AAV of Ef1a-DIO-C1V1-YFP was injected in the substantia nigra pars compacta (SNC) (AP: -3.1mm, ML: ± 1.5mm, and DV: -4.0mm) in TH-Cre mice (B6.FVB(Cg)-Tg(TH-cre)Fl172Gsat/Mmucl, MMRRC). In Figures 6 and 7 and S6I-L, the AAVs of

hSyn-DA1m/DA1h/DA1h-mut were injected into NAc (Coordinates: (AP: -1.40 mm, ML: 1.00 mm, DV: 3.90 mm)) of wild-type C57/BL6 mice (Beijing Vital River Laboratory/Charles River Laboratories) unilaterally with ~300-500 nL per animal. In Figures S6A–S6H, the AAV of hSyn-DA1h was injected into NAc (Coordinates: (AP: -1.40 mm, ML: 1.00 mm, DV: 3.90 mm)), and the AAV of hSyn-Flex-ChrimsonR-tdTomato was injected into the VTA (Coordinates: (AP: -3.28 mm, ML: 0.5 mm, DV: 4.0 mm)) of DAT-IRES-Cre mice (Jackson Laboratory).

### Fluorescence imaging of cultured cells

Imaging was performed using an inverted Ti-E A1 confocal microscope (Nikon) and the Opera Phenix high content screening system (PerkinElmer). The Nikon confocal microscope was equipped with a  $40 \times /1.35$  NA oil immersion objective, a 488-nm laser and a 561-nm laser. During imaging, the cultured cells were bathed or perfused in a chamber with Tyrode's solution containing (in mM): 150 NaCl, 4 KCl, 2 MgCl<sub>2</sub>, 2 CaCl<sub>2</sub>, 10 HEPES and 10 glucose (pH 7.4). Solutions containing the drug/compound of interest (DA (Sigma-Aldrich), Halo (Tocris), SCH 23390 (Tocris), Etic (Tocris), L-DOPA (Abcam), 5-HT (Tocris), histamine (Tocris), Glu (Sigma-Aldrich), GABA (Tocris), Ado (Tocris), ACh (Solarbio), NE (Tocris), Tyr (Sigma-Aldrich), Oct (Tocris)) were delivered via a custom-made perfusion system or via bath application. The chamber was fully cleaned with Tyrode's solution and 75% ethanol between experiments. The GFP signals (e.g., the GRAB<sub>DA</sub> sensors, the pHluorin-D<sub>2</sub>R, the iGluSnFR or EGFP-CAAX) were recorded using a 525/50-nm emission filter, and the RFP signals were collected using a 595/50-nm emission filter. The photostability was measured under 1-photon illumination (confocal microscopy) using a 488-nm laser with the laser power of ~350  $\mu$ W and the intensity of  $\sim 1.75 \times 10^2$  W/cm<sup>2</sup>, and under 2-photon illumination using a 920-nm laser with the laser power of ~27.5 mW and the intensity of  $\sim 1.375 \times 10^4$  W/cm<sup>2</sup>. Photobleaching was applied to the entire sensor-expressing HEK293T cell with the area of  $\sim 200 \mu\text{m}^2$ . The Opera Phenix high content screening system was equipped with a  $60 \times /1.15$  NA water immersion objective, a 488-nm laser, and a 561-nm laser. The GRAB<sub>DA</sub> signals were collected using a 525/50-nm emission filter, and the mCherry signals were collected using a 600/30-nm emission filter. Where indicated, the culture medium was replaced with 100  $\mu\text{l}$  of Tyrode's solution containing various concentrations of the indicated drug/compound. The fluorescence intensities of the GRAB<sub>DA</sub> sensors were calibrated using mCherry as the reference.

### cAMP-dependent reporter gene assay

The assay was performed to compare forskolin-induced cAMP levels in WT-D<sub>2</sub>R- or GRAB<sub>DA</sub>-expressing cells in response to DA application. The DA1h- or D<sub>2</sub>R-expressing cell line was transfected with the plasmid encoding the luciferase under the control of a cAMP response element. The culture medium was replaced to new culture medium before the experiment. DA was then applied to the cells to a final concentration of 100  $\mu\text{M}$ . After 15 min, culture medium containing forskolin (Sigma-Aldrich) was applied to a final concentration of 10  $\mu\text{M}$  to elevate the cAMP level. The same amount of culture medium was added to the control group. The cells were then cultured for 6 hours to enable the expression of the luciferase. Furimazine (NanoLuc Luciferase Assay, Promega) was then applied to a final concentration of 5  $\mu\text{M}$  and the luminescence was measured by VICTOR X5 multilabel plate reader (PerkinElmer).

### GTP- $\gamma$ -S binding assay

DA1m- or DA1h-IRES-mcherry-CAAX was expressed in HEK293T cells for over 24 hours in poly-D-lysine pre-coated 96-well plates and the medium was replaced by 100  $\mu\text{l}$  of Tyrode's solution before experiments. Cells were subsequently incubated with 50  $\mu\text{g}/\text{ml}$  digitonin (Sigma-Aldrich) for 5 min to permeabilize the cell membrane and washed for 2 times with 100  $\mu\text{l}$  Tyrode's solution. Tyrode's solution containing 100  $\mu\text{M}$  GTP- $\gamma$ -S (Sigma-Aldrich) was applied to the permeabilized cells in the experimental group and the cells were incubated for 10 min. The GRAB<sub>DA</sub> signals and the membrane-localized RFP signals of both the experimental group and the control group were collected by Opera Phenix high content screening system (PerkinElmer) mentioned above, before and after, various concentration of DA (ranging from 0.01 nM to 1  $\mu\text{M}$ ) was applied.

### Tango assay

DA of various concentration (ranging from 0.1 nM to 3.1  $\mu\text{M}$ ) was applied to D<sub>2</sub>R- or DA1h-expressing luciferase reporter cell lines stably expressing a tTA-dependent luciferase reporter and a  $\beta$ -arrestin2-TEV fusion gene (Kroese et al., 2015). The cells were then cultured for 12 hours to enable the expression of the luciferase. Furimazine (NanoLuc Luciferase Assay, Promega) was then applied to a final concentration of 5  $\mu\text{M}$  and the luminescence was measured by VICTOR X5 multilabel plate reader (PerkinElmer).

### Fluorescence imaging of GRAB<sub>DA</sub> in brain slices

Adeno-associated viruses (AAVs) carrying either DA1m or DA1h were injected into the nucleus accumbens (NAc) of mice and acute brain slices containing NAc were prepared two weeks later. Two weeks after the virus injection, the animals were anesthetized with IP injection of Aveton (250mg/kg) and then decapitated. The brains were removed immediately and placed directly in cold slicing buffer containing (in mM): 110 choline-Cl, 2.5 KCl, 1.25 Na<sub>2</sub>PO<sub>4</sub>, 25 NaHCO<sub>3</sub>, 7 MgCl<sub>2</sub>, 25 glucose, and 2 CaCl<sub>2</sub>. The brains were then sectioned into 200- $\mu\text{m}$  thick slices using a VT1200 vibratome (Leica), and the sections were transferred into the oxygenated Ringer's buffer containing (in mM): 125 NaCl, 2.5 KCl, 1.25 Na<sub>2</sub>PO<sub>4</sub>, 25 NaHCO<sub>3</sub>, 1.3 MgCl<sub>2</sub>, 25 glucose, and 2 CaCl<sub>2</sub>. The slices were then allowed to recover in 34°C for at least 40 min. For fluorescence imaging, the slices were transferred to an imaging chamber in an FV1000MPE two-photon microscope (Olympus) equipped with a  $40 \times /0.80$  NA water-immersion objective and a mode-locked

Mai Tai Ti: Sapphire laser (Spectra-Physics) tuned to 920 nm for the excitation of GRAB<sub>DA</sub> sensors and a 495~540-nm filter for signal collection. For electrical stimulation, a concentric electrode (model #CBAEC75, FHC) was positioned near the NAc core under the fluorescence guidance, and the imaging and stimulation were synchronized using an Arduino board with custom programs. The stimulation voltage was set at 5-6 V except for minimal stimulation experiments, and the duration of each stimulation pulse was typically set at 2 ms (1 ms for minimal stimulation experiments).

For immunostaining of brain sections, GRAB<sub>DA</sub>-expressing mice or non-injection control C57/BL6 mice were anesthetized with Avetin, and the heart was perfused with 0.9% NaCl followed with 4% paraformaldehyde (PFA). The brain was then removed and placed in 4% PFA for 4 hour, then cryoprotected in 30% (w/v) sucrose for 24 hour. The brain was embedded into tissue-freezing medium, and 50-μm-thick coronal sections were cut using a CM1900 cryostat (Leica). To label GRAB<sub>DA</sub> and dopaminergic neurons in VTA and NAc, tissue sections were rinsed and then immunostained with chicken anti-GFP antibody (1:500, Abcam, Cat#ab13970) and rabbit anti-TH antibody (Millipore, Cat#ab152, 1:500 for VTA slices and 1:100 for NAc slices), followed by the Alexa 488-conjugated goat-anti-chicken (1:200, Invitrogen, Cat#A11039) and Alexa-555-conjugated goat-anti-rabbit (1:200, AAT-Bio, Cat#16690) secondary antibodies. The immunostained tissue sections were imaged using the same Nikon confocal microscope used in cell imaging.

### Fluorescence imaging of transgenic flies

Adult *Drosophila* (within 3 weeks after eclosion) were used for imaging experiments. The fly was mounted on a customized chamber by tape, in a way the antenna and abdomen exposed to the air. A section of rectangular cuticle between the eyes, as well as air sacs and fat bodies were removed to expose the brain, which was bathed in saline, the so called adult hemolymph-like solution (AHLS): (in mM) 108 NaCl, 5 KCl, 5 HEPES, 5 Trehalose, 5 sucrose, 26 NaHCO<sub>3</sub>, 1 NaH<sub>2</sub>PO<sub>4</sub>, 2 CaCl<sub>2</sub> and 1~2 MgCl<sub>2</sub>. The same Olympus two-photon microscope used for brain slices imaging was also used here. For DA1m imaging, 920-nm excitation laser and 495~540-nm filter were used. For two-color imaging with DA1m and jRCaMP1a, 1000-nm excitation laser, 495~540-nm filter and 575~630-nm filter were used. For odor stimulation, the odorant isoamyl acetate (Sigma-Aldrich, Cat#306967) was first diluted by 200-fold in mineral oil in a bottle and second diluted by 5-fold in air, which was then delivered to the fly's antenna at a rate of 1000 ml/min. Compounds such as Halo (Tocris) and cocaine (Qinghai Pharmaceuticals) were added directly to the AHLS to their final concentration, and the following experiments were performed 10 min after compound application. For electrical stimulation, a glass electrode (resistance ~0.2 MΩ) was placed in the region of the DANs in the MB and the stimulation voltage was set at 20~80 V. For body shock, two wires were attached to the abdomen of flies, and 60 V electrical pulses were delivered for 500 ms during stimulation. For DA perfusion, a patch of blood-brain-barrier of fly was carefully removed by tweezers, and AHLS containing 100 μM DA was delivered to the brain to exchange normal bath solution. Arduino was used to synchronized stimulation delivery and imaging with custom code. The sampling rates during odor stimulation, electrical stimulation, body shock and DA perfusion were 2.7 Hz, 12 Hz, 7 Hz and 0.5 Hz respectively.

### Fluorescence imaging of zebrafish

All experiments were performed on 5 days-post-fertilization (dpf) larvae in 10% Hank's solution containing (in mM): 140 NaCl, 5.4 KCl, 0.25 Na<sub>2</sub>HPO<sub>4</sub>, 0.44 KH<sub>2</sub>PO<sub>4</sub>, 1.3 CaCl<sub>2</sub>, 1.0 MgSO<sub>4</sub>, and 4.2 NaHCO<sub>3</sub> (pH 7.2). Imaging of Tg (elval3; DA1m, DAT: TRPV1-TagRFP) larvae at 5-dpf was performed with an FV3000 inverted confocal microscope (Olympus) by using a 30X oil-immersion objective (1.05 NA, morphology imaging) or an FV1000 upright confocal microscope (Olympus) by using 40X water-immersion objective (0.8 NA, time-lapse imaging). After the larvae were paralyzed with α-bungarotoxin (100 μg/ml, Tocris), they were mounted dorsal side up in 1.5% low melting-point agarose (Sigma-Aldrich) and then immersed in an extracellular solution consisting of (in mM): 134 NaCl, 2.9 KCl, 4 CaCl<sub>2</sub>, 10 HEPES and 10 glucose (290 mOsmol/L, pH 7.8). To image the sensor expression pattern, images were acquired with a field of view consisting of 1,024 × 1,024 pixels with spatial resolution of 0.414 × 0.414 × 1 μm<sup>3</sup> (x × y × z). For bath application of compounds, DA (100 μM in 1 mM ascorbic acid solution, Sigma-Aldrich) was added by pipette at ~4 min and Halo (50 μM in DMSO, Tocris) at ~12 min. These images were acquired with a view field of 640 × 640 pixels with spatial resolution of 0.497 × 0.497 μm<sup>2</sup> (x × y) at ~1.5 Hz. For functional imaging, small anterior dissections initiated in ventricles were made, after that a glass pipette containing the TRPV1 agonist capsaicin (50 μM in absolute ethanol, Tocris) was advanced through the incision and placed near the cell bodies of the DANs. To activate the DANs, 5 pulses of puffs (9–10 psi, 100 ms) were delivered with 1-min interval. The larvae were bath in Halo (50 μM in DMSO, Tocris) for 10 min before imaging. For visual stimulation, red expanding dots were chosen in case of spectral interference. The visual stimulation was given for 3 s with ~2-min interval. These images were acquired with a field of view consisting of 800 × 800 pixels with spatial resolution of 0.397 × 0.397 μm<sup>2</sup> (x × y) at ~1 Hz.

### Fiber Photometry recording in freely moving mice

In all-optic experiments in Figure 5, optical fiber probes (105 μm core/125 μm cladding) were implanted in the dorsal striatum and in SNC 4 weeks after the virus injection. Fiber photometry recording in the dorsal striatum was performed using a 50-μW 470-nm LED, and C1V1 in the SNC was stimulated using a 9.9-mW 561-nm laser. The measured emission spectra of DA1m and tdTomato were fitted using a linear unmixing algorithm (NIH, <https://www.niehs.nih.gov/research/atniehs/labs/ln/pi/iv/tools/index.cfm>). The coefficients of DA1m and tdTomato generated by the unmixing algorithm were used to represent the fluorescence intensities of DA1m

and tdTomato, respectively (Meng et al., 2018). To evoke C1V1-mediated DA release in the dorsal lateral striatum, pulse trains (10-ms pulses at 10 Hz for 1 s) were delivered to the SNc using a 9.9-mW, 561-nm laser. In other experiments in Figures 6 and 7 and S6, an optic fiber (Thorlabs, FT200UMT, FT400UMT or BFH48-400) was attached to the implanted ferrule (Thorlabs, SF440-10) via a ceramic sleeve. A 400-Hz sinusoidal blue LED light (30 µW) (LED light: M470F1; LED driver: LEDD1B; both from Thorlabs) was band-pass filtered (passing band: 460–490 nm in Figure 6; 472 ± 15 nm, Semrock, FF02-472/30-25 in Figures 7 and S6) and delivered to the brain to excite GRAB<sub>DA</sub> sensors. The emission light then traveled through the same optic fiber, was bandpass filtered (passing band: 500–550 nm in Figure 6; 534 ± 25 nm, Semrock, FF01-535/50 in Figures 7 and S6), detected by a Femtowatt Silicon Photoreceiver (Newport, 2151) and recorded using a real-time processor (RZ2 for Figure 6; RZ5 for Figures 7 and S6; TDT). The envelope of the 400-Hz signals that reflects the intensity of the fluorescence signals was extracted in real-time using a custom TDT program.

### Behaviors

For the auditory conditioning task, mice were recovered for > 3 days after surgery, and then water-restricted until reaching 85%–90% of its original body weight and then prepared for behavior training. In the first Pavlovian task, the mice were trained on two frequency modulated pure tone auditory cues of 500 ms in duration, centered around 2.5 kHz and 11 kHz. For each mouse, one of the two tones was pseudo-randomly assigned to be the reward-predictive tone. Reward (water sweetened with 10% sucrose) was delivered through a water spout in front of the mouth following the reward-predictive cue with a variable 500–1500 ms delay. Rewarded and unrewarded trials were randomly interleaved with a variable inter-trial interval of 8–20 s. Mice experienced 200 trials (~100 rewards) per day in sessions lasting ~45 min.

In the subsequent Pavlovian conditioning task, the mice were trained on an auditory conditioning task, in which three pairs of auditory cues → outcomes pairs (or CS-US pairs; 8 kHz pure tone → 9 µl water; white noise → brief air puff to the face; and 2 kHz pure tone → no response) were delivered at random with a 10–20 s randomized inter-trial interval. The duration and intensity of each auditory cue was 1 s and 70 dB, respectively. The respective outcomes were delivered 1 s after the end of each auditory cue. The behavioral setup consisted of a custom-built apparatus allowing head fixation of the mouse's head to a Styrofoam rod (diameter: 15 cm). Rotation of the Styrofoam rod, which corresponds to the animal's running speed, was detected using an optical rotatory encoder. Licking behavior was detected when the mouse's tongue contacted the water delivery tube. Each lick signal was processed using an Arduino UNO board with custom code and sent digitally to the training program (written in MATLAB) via a serial port. Water delivery was precisely controlled using a stepping motor pump, and the air puff (15 psi, 25-ms duration) was controlled using a solenoid valve. Timing of the pump and valve was controlled using the same Arduino UNO board used for lick detection, which also provided synchronization between the training program and the TDT data acquisition system. During first two days of each training session, the outcomes were delivered without the prediction cues.

The sexual behaviors are defined following conventions in previous literature (Hull et al., 2002). DA1h was virally expressed in the NAc of male mice and an optical fiber was implanted to record the bulk fluorescence signal in freely moving animals. To confirm that DA1h can detect acute dopamine release in the NAc, Cre-dependent Chrimson-tdTomato was virally expressed in the DANs in the VTA using DAT-ires-Cre mice. Optogenetic stimulation was done three weeks after viral injection. In details, sniffing female was defined as the male's nose coming in close proximity to the female's facial, body, and/or urogenital areas. "Mount" was defined as when the male posed his forelegs over the female's back and with his hindfeet on the ground accompanying shallow pelvic thrusts. The mounting onset was defined as the moment at which the male tried to clasp female back. "Intromission" was defined as a deep rhythmic thrust following mounting. The onset of intromission was defined as the time at which the male performed the first deep thrusting toward the female with vaginal penetration. "Penile grooming" was defined when a male animal repeated grooming for his urogenital area after intromission and ejaculation. Ejaculation is detected when the male stopped thrusting and freeze for seconds. The putative ejaculation event was confirmed by the presence of vaginal copulatory plug.

### QUANTIFICATION AND STATISTICAL ANALYSIS

Image data from cultured cells, acute brain slices and transgenic flies, were first processed with ImageJ software (NIH), traces were generated by Origin 9.1 and pseudocolor images were generated by custom-written MATLAB programs. The data of electrical stimulation experiment in acute brain slices and flies were first binned by 2x and averaged to generate representative traces. The signal to noise ratio (SNR) was calculated as the peak response divided by the standard error of the baseline fluorescence fluctuation. For zebrafish-relevant data, noise reduction by a custom-written MATLAB scripts was performed. For fiber photometry experiment in Figure 6, baseline was first obtained by subtracting 2<sup>nd</sup> order exponential fitted data from the raw data after 10.17 Hz binning, and the fluorescence responses were indicated by Z score. The response to the CS was defined as the peak of the normalized PSTH between the CS onset and the US onset, and the response to US was calculated similarly using data from the US onset to data collected 2 s after the US onset. For fiber photometry experiment in Figures 7 and S6, the signal baseline was first obtained by the MATLAB function "msbackadj" with a moving window of 25% of the total recording duration. The fluorescence responses were calculated as  $(F_{\text{raw}} - F_{\text{baseline}})/F_{\text{baseline}}$ . To analyze event-evoked changes in DA release, we aligned each trial to the onset or offset of the behavior, and calculated the peri-stimulus time histogram (PSTH). To compare PSTH changes during different phases of the training, we used data from the 2<sup>nd</sup> day as naive, the 5–10<sup>th</sup> day as trained and > 10<sup>th</sup> day as well-trained, and normalized the

PSTH of each animal by water-evoked response during early training. The peak response during a behavior was calculated as the maximum  $\Delta F/F_0$  during the behavior minus the average  $\Delta F/F_0$  in the 2 s prior to the behavior onset.

Group differences were analyzed using the Student's t test, sign-rank test, One-Way ANOVA or post hoc Tukey's test. Except where indicated otherwise, all summary data presented as the mean  $\pm$  SEM.

#### **DATA AND SOFTWARE AVAILABILITY**

The self-written MATLAB, Arduino and TDT programs will be provided upon request to the Lead Contact.

# Supplemental Figures

Cell

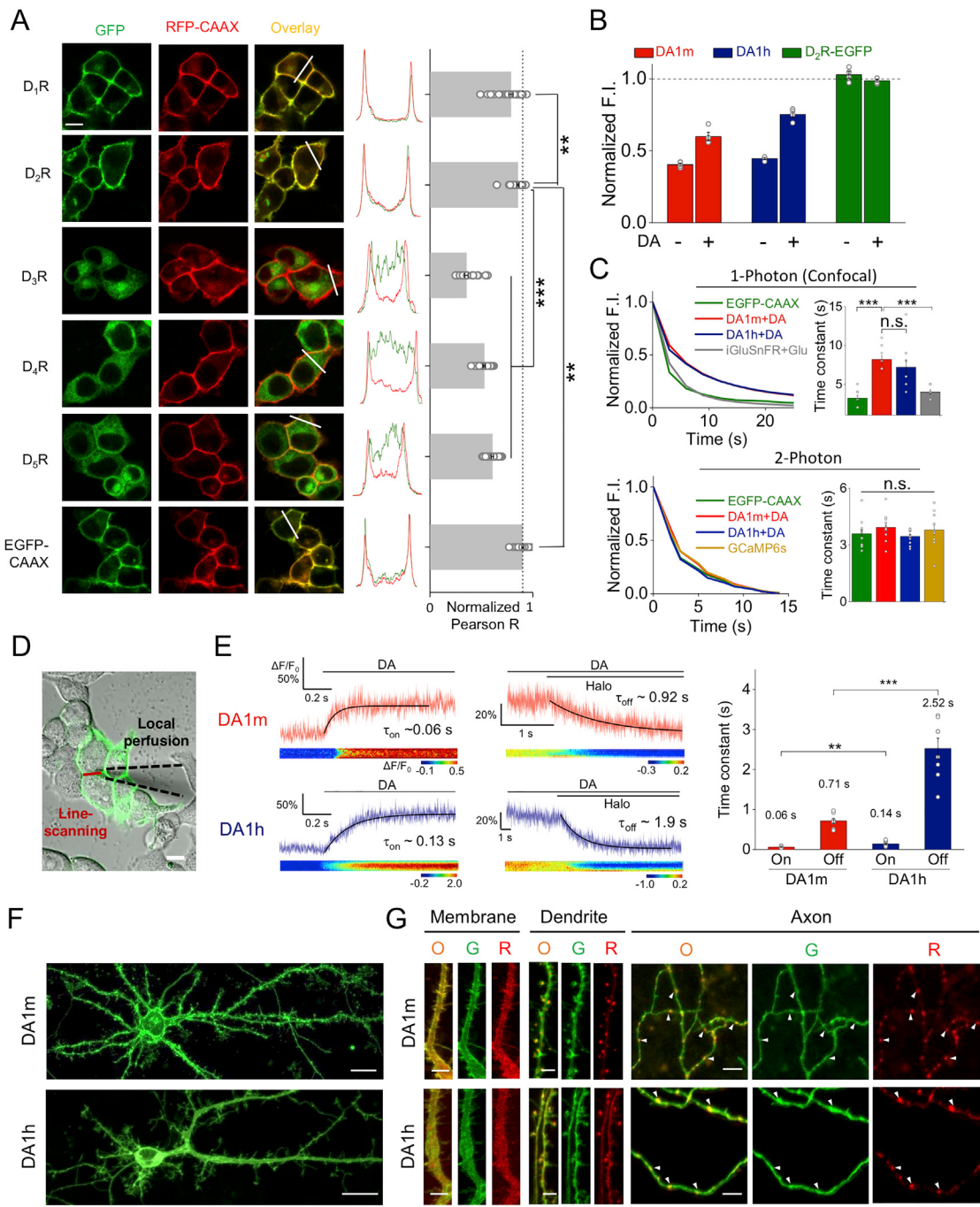


**Figure S1. Screening and Characterization of GRAB<sub>DA</sub> Sensors in HEK293T Cells or Neurons, Related to Figure 1**

(A) The fluorescence and membrane trafficking of all five DRs with cpEGFP insertion. A membrane-localized RFP (RFP-CAAX) was co-expressed to indicate the plasma membrane and EGFP-CAAX was used as a control. Left, the fluorescence images of HEK293T cells expressing all five DR-based chimeras or EGFP-CAAX (green) and RFP-CAAX (red); scale bar, 10  $\mu$ M; white bars in overlay panels, line-scanning region. Middle, the normalized line-scanning plots of the fluorescence signals in both green and red channels. Right, Pearson's colocalization ratios of the DR-based chimeras or EGFP-CAAX according to RFP-CAAX ( $n = 30/2$  for each protein;  $p < 0.001$  comparing D<sub>2</sub>R with D<sub>3</sub>R, D<sub>4</sub>R and D<sub>5</sub>R;  $p = 0.001$  between D<sub>2</sub>R and EGFP-CAAX;  $p = 0.006$  between D<sub>2</sub>R and D<sub>1</sub>R).

(B) Relative brightness of DA1m and DA1h compared with D<sub>2</sub>R-EGFP chimeric construct in the absence and presence of 100  $\mu$ M DA ( $n = 4$  wells/group with 100–200 cells/well).

(C) Photostability of DA1m and DA1h compared with other fluorescent probes. Top: Representative photobleaching curves of DA1m, DA1h, EGFP-CAAX and iGluSnFR expressed in HEK293T cells under confocal imaging (488 nm laser with the laser power of ~350  $\mu$ W and the intensity of  $\sim 1.75 \times 10^2$  W/cm<sup>2</sup>) are shown in left. The group data of decay time constants of each are shown in right ( $n = 10/3$  of each group;  $p = 0.350$  between DA1m and DA1h;  $p < 0.001$  comparing DA1m

(legend continued on next page)

with EGFP-CAAX and iGluSnFR). Bottom: Similar as top, except that two-photon laser (920nm laser with the laser power of ~27.5 mW and the intensity of  $\sim 1.38 \times 10^4 \text{ W/cm}^2$ ) was used to test the photostability of DA1m, DA1h, EGFP-CAAX and GCaMP6s ( $n = 12/2$  of each group;  $p = 0.251$  between EGFP-CAAX and DA1m;  $p = 0.583$  between EGFP-CAAX and DA1h;  $p = 0.537$  between EGFP-CAAX and GCaMP6s;  $p = 0.051$  between DA1m and DA1h;  $p = 0.678$  between DA1m and GCaMP6s;  $p = 0.236$  between DA1h and GCaMP6s).

(D) Schematic image showing the rapid local perfusion system. A glass pipette (black dashed lines) filled with DA or Halo was positioned close to the GRAB<sub>DA</sub>-expressing cells, and fluorescence signals were measured using confocal line-scanning (red line).

(E) Left and middle: Representative fluorescence changes in GRAB<sub>DA</sub>-expressing cells in response to the local perfusion (on rate: 100  $\mu\text{M}$  DA in pipette with normal bath solution; off rate: 1 mM Halo in pipette with bath solution containing 10  $\mu\text{M}$  DA for DA1m or 1  $\mu\text{M}$  DA for DA1h). The traces are the average of 3 different ROIs on the scanning line, shaded with  $\pm$  SEM and fitted with a single-exponential function (black traces, with the decay time constants shown). Right: Group data summarizing the response kinetics of GRAB<sub>DA</sub>-expressing cells in response to DA (on) or Halo (off) ( $n = 8$  cells/group;  $p = 0.0093$  between on kinetics;  $p < 0.001$  between off kinetics).

(F) Expression of GRAB<sub>DA</sub> sensors in cultured neurons. Scale bars, 20  $\mu\text{m}$ .

(G) Expression and localization of GRAB<sub>DA</sub> sensors (green, G), subcellular markers (red, R) and the overlay (O) in the indicated subcellular compartments in cultured neurons. RFP-CAAX, PSD95-RFP and Synaptophysin-RFP were co-expressed as markers of the plasma membrane, dendritic spines, and presynaptic boutons, respectively. Arrow heads indicate synaptic boutons. Scale bars, 5  $\mu\text{m}$ .

Values with error bars indicate mean  $\pm$  SEM. Student's t test performed; n.s., not significant; \*\* $p < 0.01$ ; \*\*\* $p < 0.001$ .

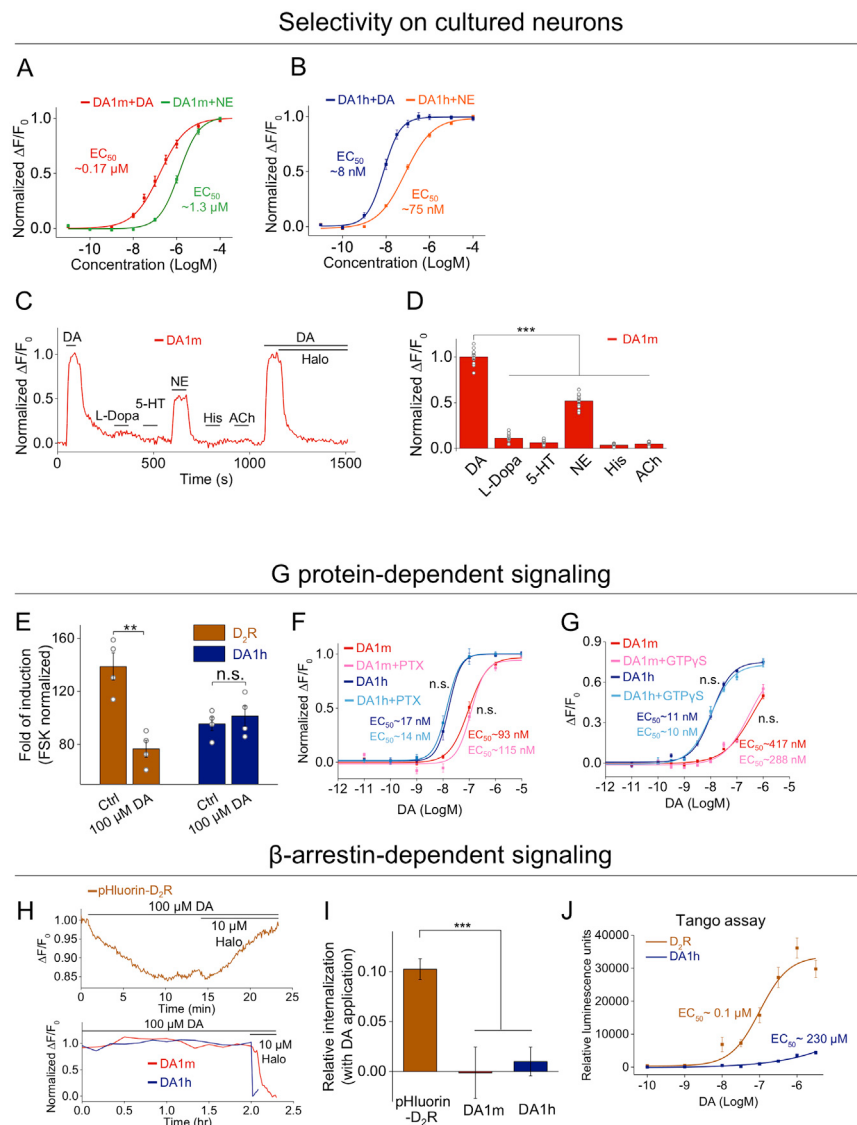


**Figure S2. Selectivity to DA and NE, as well as the Efficacy Coupling Downstream Signaling of DA1m/h-Expressing HEK293T Cells or Cultured Neurons, related to Figure 1**

(A and B) Normalized dose-dependent fluorescence responses to DA and NE of DA1m- (A) or DA1h- (B) expressing cultured neurons (DA1m+DA: n = 10/6; DA1m+NE: n = 12/5; DA1h+DA: n = 10/5; DA1h+NE: n = 11/8).

(C and D) Representative trace (C) and group analysis (D) of the fluorescence changes of DA1m-expressing neurons in response to the sequential application of the indicated compounds at 1 μM, including DA, L-Dopa, 5-HT, NE, His, ACh, DA(<sup>2nd</sup>) and DA+Halo (n = 12/12; p < 0.001 comparing responses to DA with L-Dopa, 5-HT, NE, His, ACh and DA+Halo).

(E) Fold of induction, which revealed the cAMP level, in the luciferase assay of D<sub>2</sub>R- (brown) or DA1h- (blue) expressing Nanoluc reporter cells bathed in control normal solution or solution containing 100 μM DA (n = 4 wells/group; p = 0.002 for D<sub>2</sub>R; p = 0.544 for DA1h).

(F) Normalized fluorescence changes in GRAB<sub>DA</sub>-expressing cells in response to the application of DA, with or without the co-expression of pertussis toxin (PTX) (DA1m: n = 14/3; DA1m+PTX: n = 14/3; DA1h: n = 10/3; DA1h+PTX: n = 10/3; p = 0.680 comparing the EC<sub>50</sub> of DA1m and DA1m+PTX; p = 0.810 comparing the EC<sub>50</sub> of DA1h and DA1h +PTX).

(G) Fluorescence changes in GRAB<sub>DA</sub>-expressing cells in response to the application of DA, with or without the pre-bathing of GTPγS (n = 3 well/group with 100–300 cell/well; p = 0.488 comparing the EC<sub>50</sub> of DA1m and DA1m+GTPγS; p = 0.474 comparing the EC<sub>50</sub> of DA1h and DA1h+GTPγS).

(H) Top: The representative trace of the total fluorescence changes in pHluorin-D<sub>2</sub>R-expressing HeLa cells in response to the application of 100 μM DA followed by 10 μM Halo. Bottom: Exemplar traces of normalized fluorescence changes of DA1m- (red) and DA1h- (blue) expressing neurons during a 2-hour application of 100 μM DA.

(I) Quantification of relative internalization of pHluorin-D<sub>2</sub>R, DA1m and DA1h in response to the application of 100 μM DA (pHluorin-D<sub>2</sub>R: n = 12/2; DA1m: n = 20/12; DA1h: n = 14/6).

(J) Dose-dependent luminescence units in the tango assay of D<sub>2</sub>R- (brown) or DA1h- (blue) expressing cells in response to DA application (n = 3 well/group with 100–300 cell/well).

Values with error bars indicate mean ± SEM. Student's t test performed; n.s., not significant; \*\*p < 0.01; \*\*\*p < 0.001.

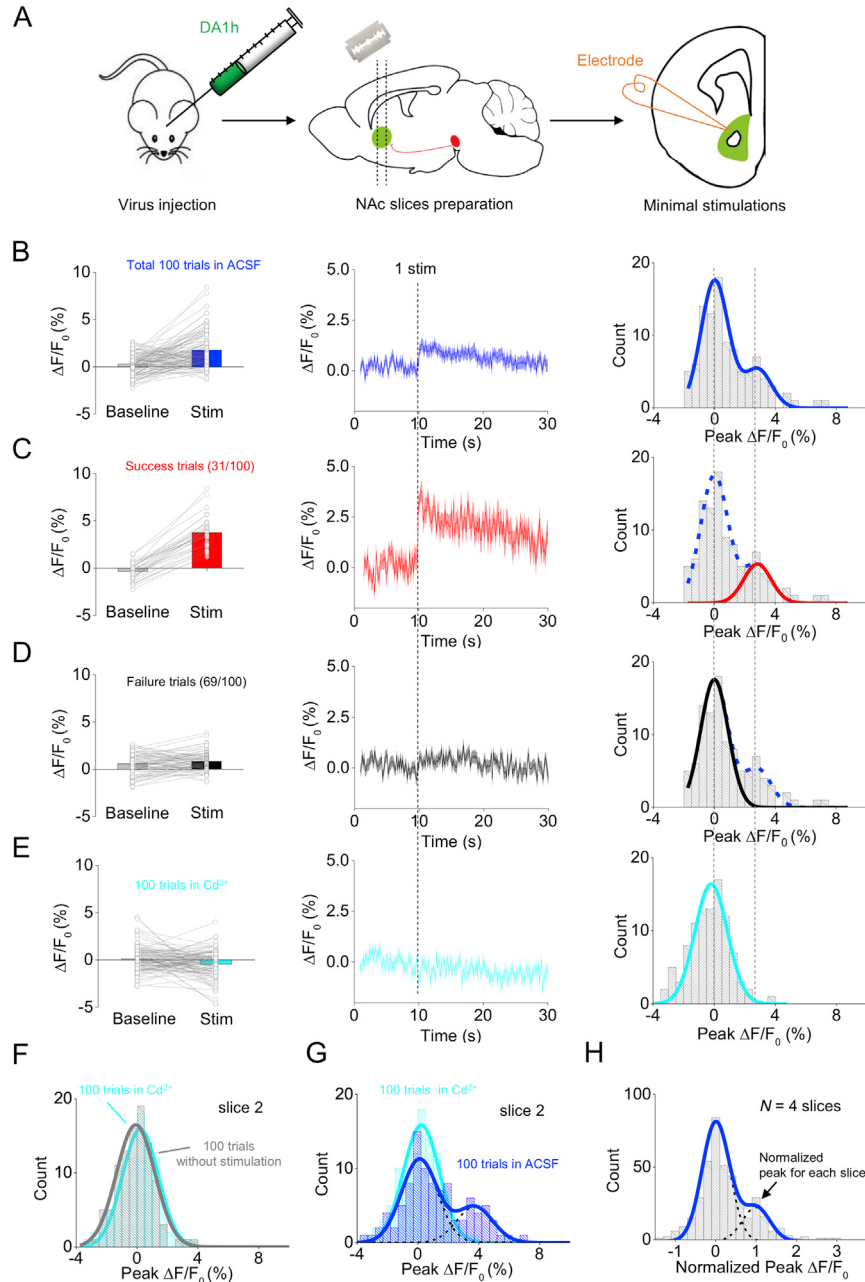


**Figure S3. GRAB<sub>DA</sub> Sensors Report Minimal Stimulation-Induced DA Release in NAc Slices, Related to Figure 2**

(A) Schematic illustration of the DA1h virus injection, NAc slice preparation and minimal electrical stimulation in mice.

(B–D) Left, the fluorescence responses of DA1h-expressing neurons before (baseline) and after stimulation (stim) in a total of 100 trials under minimal stimulation condition (B), of which 31 trials were successes (C) and 69 trials were failures (D). The  $\Delta F/F_0$  of 3 frames before stimulation and immediately after stimulation were averaged as “baseline” and “stim.” Middle, the averaged fluorescence traces of all 100 trials (B), of 31 success trials (C), of 69 failure trials (D). Right, the distribution of peak  $\Delta F/F_0$  of all 100 trials (B, blue), with success trials highlighted in (C, red) and failure trials highlighted in (D, black).

(E) Similar as (B), except that ACSF containing 200  $\mu$ M  $Cd^{2+}$  was bathed to the same slice.

(F) A different DA1h- expressing slice where distributions of peak  $\Delta F/F_0$  in 100 minimal stimulation trials in ACSF (gray) and in ACSF containing  $Cd^{2+}$  (light blue) were compared.

(G) Similar as (F), except the distributions of peak  $\Delta F/F_0$  in ACSF (blue) and ACSF containing  $Cd^{2+}$  (light blue) were compared.

(H) Distribution of the group data under minimal stimulation, where peak  $\Delta F/F_0$  from individual DA1h- expressing slices was normalized and pooled together (~400 stimulation trials in total from 4 slices of 3 mice). Note, the normalization was done by first fitting for each set of data to identify the peak of failures as “zero” and peak of success as “one”.

Values with error bars indicate mean  $\pm$  SEM.

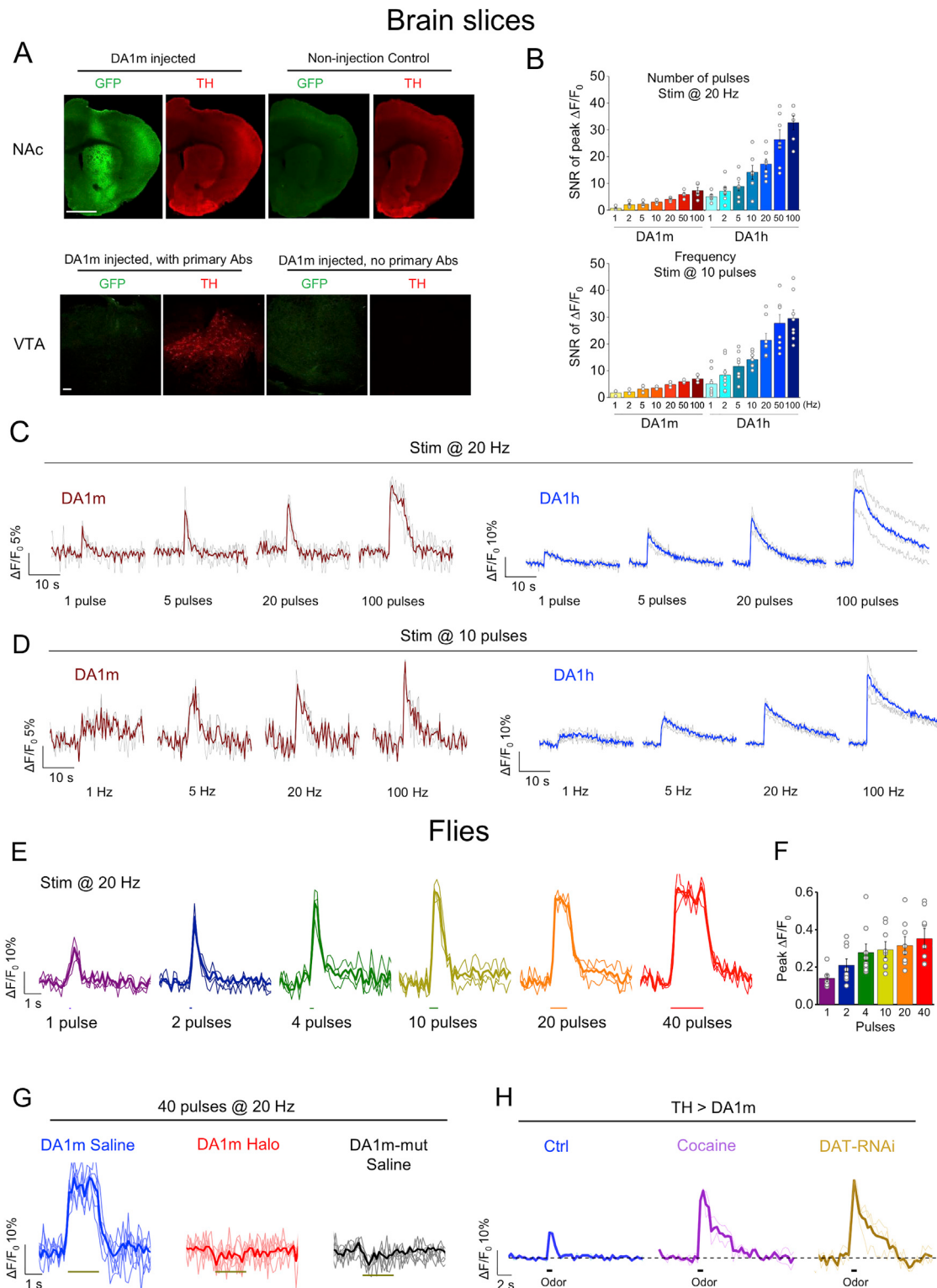
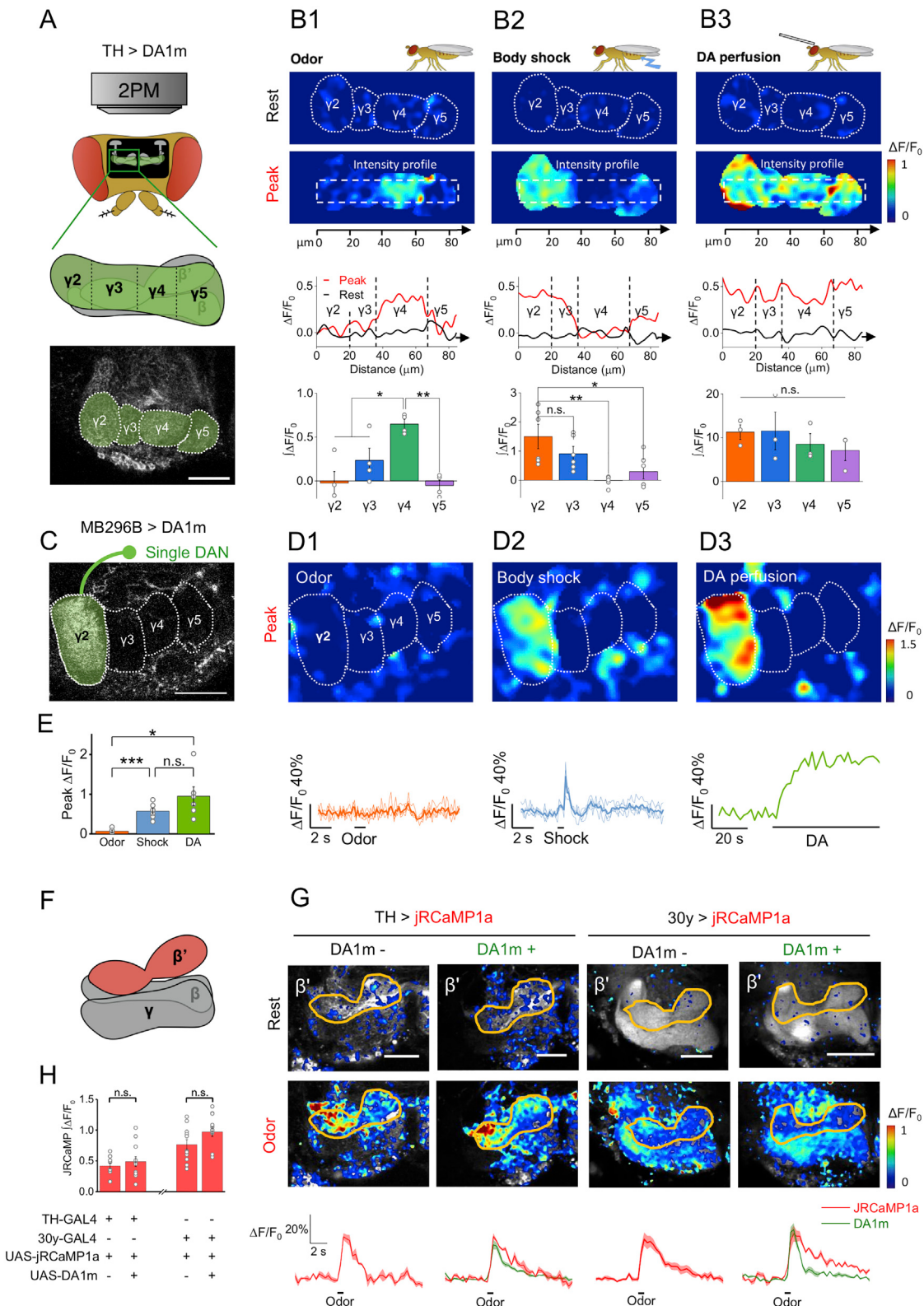


**Figure S4. The Single-Trial Data of DA1m Fluorescence Responses in NAc Brain Slices and Flies, Related to Figures 2 and 3**

(A) Top: representative immunoreactive signals of GFP (green) and TH (red) in NAc slices of DA1m injected mice (left) or non-injection control mice (right). Scale bar, 1mm.

(legend continued on next page)

- 
- Bottom: representative immunoreactive signals of GFP (green) and TH (red) in VTA slices of DA1m injected mice with (left) or without (right) the application of primary antibodies. Scale bar, 10  $\mu$ m.
- (B) Group analysis of the signal-to-noise ratio (SNR) of the fluorescence responses of DA1m- or DA1h-expressing neurons to a trial of electrical stimuli at different pulse numbers (left, n = 5 slices from 3 mice in DA1m; n = 7 slices from 4 mice in DA1h), or a trial of 10-pulse electrical stimuli with different frequencies (right, n = 3 slices from 2 mice in DA1m; n = 5–8 slices from 3 mice in DA1h).
- (C) Three single trials (gray) and corresponding averaged trials (red in DA1m, blue in DA1h) of fluorescence responses of DA1m- or DA1h-expressing neurons to a train of 20-Hz electrical stimuli containing the indicated pulse numbers.
- (D) Similar as in (C) except that a train of 10-pulse electrical stimuli at the indicated frequencies was applied.
- (E and F) Fluorescence changes of TH > DA1m flies in response to electrical stimuli with indicated pulses at 20 Hz. Representative 3 single trial traces (light) with corresponding averaged traces (bold) from one fly are shown in (E). Group data of peak  $\Delta F/F_0$  are summarized in (F) (n = 9 flies/group).
- (G) Fluorescence changes of TH > DA1m and TH > DA1m-mut flies in response to 40-pulse electrical stimuli at 20 Hz, in normal saline or in saline containing 10  $\mu$ M Halo. Representative 6 single trial traces (light) with corresponding averaged traces (bold) from one fly/group are shown.
- (H) Fluorescence changes of TH > DA1m flies in response to 1-s odor stimulation in control condition (left), in the presence of the DAT blocker cocaine (3  $\mu$ M, middle), or in DAT-RNAi genetic background (right). Representative 2–3 single trial traces (light) with corresponding averaged traces (bold) from one fly/group are shown.
- Values with error bars indicate mean  $\pm$  SEM.



(legend on next page)

**Figure S5. Characterization of the Spatial Resolution and Sensitivity and the Effect on  $\text{Ca}^{2+}$  Signaling of DA1m by Fly *In Vivo* Imaging, Related to Figure 3**

(A) Top panel, schematic illustration showing the TH > DA1m fly *in vivo* two-photon imaging. Bottom panels, the cartoon and the field of view indicate MB  $\gamma$ 2-5 compartments in this focal plane.

(B) Fluorescence signals of TH > DA1m fly in response to 1-s odor, 500-ms body shock and 100  $\mu\text{M}$  DA perfusion. Representative pseudocolor images and corresponding intensity profiles from one fly are shown in top and middle panels. Group data are summarized in bottom panels ( $n = 4$  flies for odor;  $n = 6$  flies for body shock;  $n = 3$  flies for DA perfusion; for odor, comparing  $\gamma$ 4 with  $\gamma$ 2,  $\gamma$ 3 and  $\gamma$ 5,  $p = 0.011, 0.027$  and  $0.002$ ; for body shock, comparing  $\gamma$ 2 with  $\gamma$ 3,  $\gamma$ 4 and  $\gamma$ 5,  $p = 0.211, 0.009$  and  $0.027$ ; for DA perfusion,  $p = 0.967$  between  $\gamma$ 2 and  $\gamma$ 3,  $p = 0.284$  between  $\gamma$ 2 and  $\gamma$ 4;  $p = 0.305$  between  $\gamma$ 2 and  $\gamma$ 5;  $p = 0.131$  between  $\gamma$ 3 and  $\gamma$ 4;  $p = 0.282$  between  $\gamma$ 3 and  $\gamma$ 5;  $p = 0.944$  between  $\gamma$ 4 and  $\gamma$ 5).

(C) Schematic illustration and the field of view depicting the expression of DA1m in single DAN each hemisphere driven by MB296B-GAL4.

(D and E) Fluorescence signals of MB296B > DA1m fly in response to 1-s odor, 500-ms body shock and 100  $\mu\text{M}$  DA perfusion. Representative pseudocolor images (averaged from 3 trials) and corresponding traces (light, 3 single trial traces; bold, 3-trial averaged traces) from one fly are shown in (D). The group analysis of peak  $\Delta F/F_0$  are summarized in (E) ( $n = 5$  flies for odor;  $n = 6$  flies for body shock;  $n = 6$  flies for DA perfusion;  $p < 0.001$  between sham and body shock;  $p = 0.013$  between sham and DA perfusion;  $p = 0.178$  between body shock and DA perfusion).

(F) Schematic illustration of the MB  $\beta'$  lobe.

(G and H) Fluorescence responses of jRCaMP1a- and DA1m-expressing DANs (left) or Kenyon cells (right) to 1-s odor stimulation. Representative pseudocolor images and corresponding 3-trial-averaged traces shaded with  $\pm$  SEM from one fly are shown in (G). Group data of the integrals of jRCaMP1a signals are summarized in (H) (TH > jRCaMP1a:  $n = 10$  flies; TH > jRCaMP1a, DA1m:  $n = 11$  flies; 30y > jRCaMP1a:  $n = 11$  flies; 30y > jRCaMP1a, GRAB<sub>DA1m</sub>:  $n = 12$  flies;  $p = 0.503$  between TH > jRCaMP1a and TH > jRCaMP1a, DA1m;  $p = 0.097$  between 30y > jRCaMP1a and 30y > jRCaMP1a, DA1m).

Scale bars in (A), (C), and (G) are 25  $\mu\text{m}$ . Values with error bars indicate mean  $\pm$  SEM. Student's t test performed; n.s., not significant; \* $p < 0.05$ ; \*\* $p < 0.01$ ; \*\*\* $p < 0.001$ .

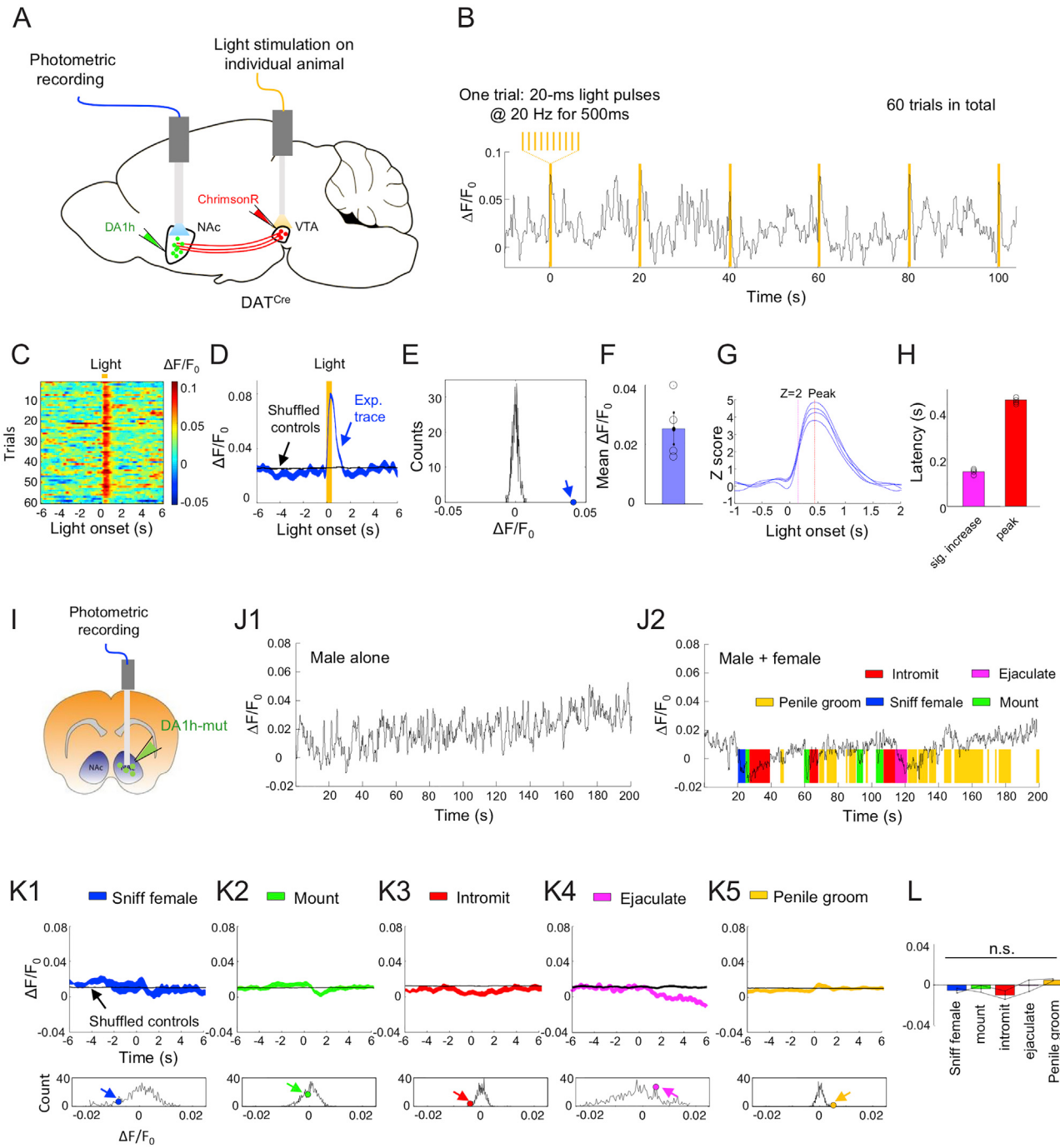


**Figure S6. Fluorescence Signals of DA1h in NAc Evoked by Optogenetically Stimulation of DANs in VTA and Signals of DA1h-mut in NAc during Male Sexual Behaviors, Related to Figure 7**

(A) Schematic diagram showing the experimental design used to record DA1h signals in the NAc (AAV hsyn-DA1h) while optogenetically activating the VTA DANs (AAV hsyn-Flex-ChrimsonR-tdTomato). 593-nm 20-ms yellow light was delivered at 20 Hz for 500 ms in each trial, and 60 trials were applied with 20-s interval to one animal.

(B-E) Representative fluorescence changes during optogenetic stimulations from one mouse. (B) Snapshot of 6 trials. (C) Heatmap showing all 60-trial fluorescence signals aligned to the light onset. (D) Post-event histogram (PETH) showing the averaged fluorescence changes of 60-trial light stimulation (blue) and 1000 × shuffled controls (black). Shaded represent  $\pm$  SEM. (E) The distributions of mean  $\Delta F/F_0$  of shuffled controls. The colored dot and arrow indicate the actual mean  $\Delta F/F_0$  during the light stimulation.

(F) Group data summarizing the mean  $\Delta F/F_0$  increase during light stimulation ( $n = 4$  animals). Error bar:  $\pm$  SEM. Student t test is performed to compare the mean  $\Delta F/F_0$  of stimulation with that of shuffled controls,  $F(3) = 4.60$ ,  $p = 0.019$ .

(legend continued on next page)

(G) Z score normalized PETHs of all 4 animals aligned to the light onset. The Z score at each time point is calculated using the -6 to 0 s prior to light onset as the baseline. Magenta line indicates the average latency to reach  $Z = 2$ . Red line indicates the average latency to reach peak response.

(H) Group data summarizing the latency to reach significant increase ( $Z = 2$ ) and peak response after light stimulation.

(I) Schematic diagram showing the experimental design used to record DA1h mutant signals in the NAc (AAV hsyn-DA1h-mut) of male mice during sexual behaviors.

(J) Representative fluorescence changes right before female introduction (Ji) and during male sexual behaviors (Jii). The shaded areas with colors indicate different behavioral events.

(K) Top: PETHs showing the fluorescence changes aligned to various behavioral events. Black lines show averaged PETHs of 1000  $\times$  shuffled controls. Shaded represent  $\pm$  SEM. Bottom: The distributions of mean  $\Delta F/F_0$  of shuffled controls. Colored dots and arrows indicate the actual mean  $\Delta F/F_0$  during each behavior. Mean  $\Delta F/F_0$  is calculated as averaged  $\Delta F/F_0$  from 0-1 s after the behavioral onset minus the baseline  $\Delta F/F_0$ . Baseline for sniff, mount, intromit and lick is defined as -12 to -2 s before the onset of each behavioral episode. Baseline for ejaculation is defined as 10 to 20 s after the onset of the behavior given that ejaculation is always preceded by mounting and intromission.

(L) Group data summarizing the mean  $\Delta F/F_0$  during various behaviors of two animals. One-way ANOVA with repeated-measures. Among behaviors:  $F(3, 4) = 0.63$ .  $p = 0.473$ .

Values with error bars indicate mean  $\pm$  SEM.